Title
Nanoparticle Interactions with Lipid Bilayers

Author
Edwards, Shayson C.

Publication Date
2015

Peer reviewed|Thesis/dissertation

University of California

Los Angeles

Nanoparticle Interactions with Lipid Bilayers

A thesis submitted in partial satisfaction

of the requirements for the degree Master of Science

in Bioengineering

by

Shayson Christopher Edwards

2015

Abstract of the Thesis

Nanoparticle Interactions with

Lipid Bilayers

by

Shayson Christopher Edwards

Master of Science in Bioengineering

University of California, Los Angeles, 2015

Professor Jacob Schmidt, Chair

There are many applications for artificial lipid bilayers. These applications include ion channel studies, protein sensing with nanopores—especially DNA sequencing, and artificial lipid bilayers have the potential be applied for use in nanoparticle toxicity screening. Arrays of bilayers were used to test different nanoparticles for interactions in a variety of different environments including changes in particle concentration, ionic strength, pH, and presence of serum. Nanoparticles which were screened for interactions and potentially toxicity with our bilayer array platform included lanthanum oxide, cerium oxide, copper oxide, cobalt oxide, zinc oxide, indium oxide, erbium oxide, europium oxide, and

gadolinium oxide. The data from our bilayer array platform also indicated that the ability of nanoparticles to destruct membranes largely depends on experimental conditions. In general, positive coating such as a low pH condition makes the particles more potent to membranes, and less positive coating such as a higher pH makes the particles more or less likely to interact and ultimately disrupt the bilayers. These results about nanoparticles' ability to disrupt and break bilayers have a strong correlation literature regarding nanoparticle toxicity. This information can be used as a platform and starting point to study and predict how other nanoparticles or drugs may interact with bilayers.

The thesis of Shayson Christopher Edwards is approved.

Benjamin M. Wu

Gerard C. L. Wong

Jacob J. Schmidt, Committee Chair

University of California, Los Angeles

2015

Dedication

I would like to dedicate this work to my parents, Karen and Steven. Thank you for your lifelong support and encouragement in all of my endeavors.

Table of Contents

Abstract of the Thesis ii

Committee iv

Dedication v

Table of Contents vi

List of Figures ix

List of Tables xiii

Acknowledgements xv

Chapter 1: Introduction 1

1.1 Introduction 1

1.2 Overview of Bilayer Creation Methods 2

1.3 Droplet Bilayers 4

1.4 Bilayer Measurements 5

1.5 Experimental Philosophy 9

Chapter 2: Multichannel Horizontal Bilayer Array 10

2.1 Overview 10

2.2 Materials 12

2.3 Chip Fabrication, Assembly, and Prep 15

2.4 Partition Quality Control 16

Chapter 3: Experimental Approach to Nanoparticles 23

3.1 Nanoparticle Overview 23

3.2 Concentration Profiles 25
3.3 Ionic Strength Profiles 26
3.4 pH Profiles 26
3.5 Serum Experiments 27
3.6 Example Results 28
Chapter 4: Nanoparticle Results & Discussion 32
4.1 Nanoparticle Results Overview 32
4.2 Lanthanum Oxide (La_2O_3) 35
4.3 Cerium Oxide (CeO_2) 40
4.4 Copper Oxide (CuO) 45
4.5 Cobalt Oxide (Co_3O_4) 49
4.6 Zinc Oxide (ZnO) 53
4.7 Indium Oxide (In_2O_3) 57
4.8 Erbium Oxide (Er_2O_3) 61
4.9 Europium Oxide (Eu_2O_3) 66
4.10 Gadolinium Oxide (Gd_2O_3) 69
Chapter 5: Future Work 74
Appendix A: Protocols 75
A.1 Neutral Super Combo and Super Combo Lipid Preparation 75
A.2 Liposome and Lipid in Oil Preparation 78
A.3 Partition Hole Size and Quality Control Protocol 80
A.4 Acrylic Chip Assembly Protocol 82

A.5 Multichannel Horizontal Bilayer Platform Protocol with Buffer Solution 84

A.6 Serum Preparation 86

A.7 Multichannel Horizontal Bilayer Platform Protocol with Serum Solution 87

A.8 Painted Bilayer Preparation and Protocol 89

References 91

List of Figures

Figure 1: Lipid Bilayer Illustration: Bilayers are composed two lipid monolayers with the hydrophilic head facing out to aqueous solution and the hydrophobic tail embedded inside away from the aqueous solution. (Figure adapted from Sundava et al.).....2

Figure 2: Painted bilayer apparatus schematic. A: Two compartments divided by Teflon® film composed of an aperture with a diameter of 50-300μm. An electrolyte solution is filled in both compartments above the aperture level. Silver chloride electrodes are connected to an amplifier and are inserted into the electrolytic solution to measure the electrical properties and characteristics of the pore. B: A cross-sectional view of the bilayer formed across the aperture. Once the bilayer has formed, a solvent annulus remains at the boundary between the bilayer and the edge of the pore. (Meyer et al.) 3

Figure 3: Folded bilayer formation. A: Bilayer formation apparatus. B: Folding two monolayers to form a bilayer. Illustrations are not to scale. (Montal and Mueller.)[19].....4

Figure 4: Example of establishing minimum current fluctuation for pore determination 8

Figure 5: Illustration of multichannel horizontal bilayer array. (Figure adapted from Lu et al.) 11

Figure 6: Acrylic sheets used for multichannel horizontal bilayer array.....13

Figure 7: Nanoparticles in raw form 14

Figure 8: Chip Assembly. From left to right: bottom tape, top tape, partition, top acrylic, bottom glued acrylic, assembled chip. 16

Figure 9: A partition exhibiting undesired characteristics. The left side of the shows signs of jaggedness, the hole itself is not symmetrical, and the hole size is much closer to 600μm than 700μm. 17
Figure 10: Partition Analysis 19
Figure 11: Laser cut partition array 21
Figure 12: Example of simple pore formations/interactions highlighted in red. Changes in current are small spikes much larger than the adjacent background noise. Spikes are short in duration. 28
Figure 13: Example of transient pore formations highlighted in red. Changes in current are small to large spikes larger magnitude in comparison adjacent background noise. Transient pore spikes are longer in duration and may be a relatively constant current during formation. 29
Figure 14: Example of voltage dependency. Current fluctuations, encapsulated in red are present on the left half of the figure, the positive applied voltage section. A lack of current fluctuations or pore formations, shown in blue, on the right half of the figure, the negative applied voltage portion of experimental protocol. 30
Figure 15: Example of a fusion event 31
Figure 16: Ionic Strength Experiment Data Summary 33
Figure 17: pH Experiment Data Summary 34
Figure 18: Serum Experiment Data Summary 35
Figure 19: Lanthanum Oxide (100 μg/ml): A: Typical trace of an experimental well with particle added. B: Typical trace of a control well with buffer added. C: Typical trace of

an interaction event in an experimental well after particle has been added. D: Typical trace of a fusion event of an experimental well after particle has been added. 37
Figure 20: Cerium Oxide (200 µg/ml): A: Typical trace of an experimental well with particle added. B: Typical trace of a control well with buffer added. C: Typical trace of an interaction event in an experimental well after particle has been added. D: Typical trace of a fusion event of an experimental well after particle has been added. 42
Figure 21: Copper Oxide (100µg/ml): A: Typical trace of an experimental well with particle added. B: Typical trace of a control well with buffer added. C: Typical trace of an interaction event in an experimental well after particle has been added. D: Typical trace of a fusion event of an experimental well after particle has been added. 46
Figure 22: Cobalt Oxide (500 µg/ml): A: Typical trace of an experimental well with particle added. B: Typical trace of a control well with buffer added. C: Typical trace of an interaction event in an experimental well after particle has been added. D: Typical trace of a fusion event of an experimental well after particle has been added. 50
Figure 23: Zinc Oxide (50 µg/ml): A: Typical trace of an experimental well with particle added. B: Typical trace of a control well with buffer added. C: Typical trace of an interaction event in an experimental well after particle has been added. D: Typical trace of a fusion event of an experimental well after particle has been added. 54
Figure 24: Indium Oxide (500 µg/ml): A: Typical trace of an experimental well with particle added. B: Typical trace of a control well with buffer added. C: Typical trace of an interaction event in an experimental well after particle has been added. D: Typical trace of a fusion event of an experimental well after particle has been added. 58

Figure 25: Erbium Oxide (100 µg/ml): A: Typical trace of an experimental well with particle added. B: Typical trace of a control well with buffer added. C: Typical trace of an interaction event in an experimental well after particle has been added. D: Typical trace of a fusion event of an experimental well after particle has been added. 63

Figure 26: Europium Oxide (100µg/ml): A: Typical trace of an experimental well with particle added. B: Typical trace of a control well with buffer added. C: Typical trace of an interaction event in an experimental well after particle has been added. D: Typical trace of a fusion event of an experimental well after particle has been added. 67

Figure 27: Gadolinium Oxide (100 µg/ml): A: Typical trace of an experimental well with particle added. B: Typical trace of a control well with buffer added. C: Typical trace of an interaction event in an experimental well after particle has been added. D: Typical trace of a fusion event of an experimental well after particle has been added. 71

List of Tables

Table 1: Lanthanum Oxide Initial Fusion Rate Experiments 36

Table 2: Lanthanum Oxide Ionic Strength Experimental Fusion Rates 38

Table 3: Lanthanum Oxide pH Range Experimental Fusion Rates 39

Table 4: Lanthanum Oxide Serum Experimental Fusion Rates 40

Table 5: Cerium Oxide Initial Fusion Rate Experiments 40

Table 6: Cerium Oxide Ionic Strength Experimental Fusion Rates 43

Table 7: Cerium Oxide pH Range Experimental Fusion Rates 44

Table 8: Cerium Oxide Serum Experimental Fusion Rates 44

Table 9: Copper Oxide Initial Fusion Rate Experiments 45

Table 10: Copper Oxide Ionic Strength Experimental Fusion Rates 47

Table 11: Copper Oxide pH Range Experimental Fusion Rates 48

Table 12: Copper Oxide Serum Experimental Fusion Rates 48

Table 13: Cobalt Oxide Initial Fusion Rate Experiments 49

Table 14: Cobalt Oxide Ionic Strength Experimental Fusion Rates 51

Table 15: Cobalt Oxide pH Range Experimental Fusion Rates 52

Table 16: Cobalt Oxide Serum Experimental Fusion Rates 52

Table 17: Zinc Oxide Initial Fusion Rate Experiments 53

Table 18: Zinc Oxide Ionic Strength Experimental Fusion Rates 55

Table 19: Zinc Oxide pH Range Experimental Fusion Rates 56

Table 20: Zinc Oxide Serum Experimental Fusion Rates 56

Table 21: Indium Oxide Initial Fusion Rate Experiments 57
Table 22: Indium Oxide Ionic Strength Experimental Fusion Rates 59
Table 23: Indium Oxide pH Range Experimental Fusion Rates 60
Table 24: Indium Oxide Serum Experimental Fusion Rates 61
Table 25: Erbium Oxide Initial Fusion Rate Experiments 62
Table 26: Erbium Oxide Ionic Strength Experimental Fusion Rates 64
Table 27: Erbium Oxide pH Range Experimental Fusion Rates 65
Table 28: Erbium Oxide Serum Experimental Fusion Rates 66
Table 29: Europium Oxide Initial Fusion Rate Experiments 66
Table 30: Europium Oxide Ionic Strength Experimental Fusion Rates 68
Table 31: Europium Oxide pH Range Experimental Fusion Rates 69
Table 32: Europium Oxide Serum Experimental Fusion Rates 69
Table 33: Gadolinium Oxide Initial Fusion Rate Experiments 70
Table 34: Gadolinium Oxide Ionic Strength Experimental Fusion Rates 72
Table 35: Gadolinium Oxide pH Range Experimental Fusion Rates 73
Table 36: Gadolinium Oxide Serum Experimental Fusion Rates 73
Table 37: Super Combo Plus BMP Lipid Composition 75
Table 38: Super Combo Lipid Composition 76
Table 39: Neutral Super Combo Lipid Composition 76

Acknowledgements

I would like to acknowledge all of the people who helped make this work a reality. I would like to thank Dr. Schmidt for allowing me to research in his lab. I appreciate Dr. Schmidt for always providing enough guidance for me in times of trouble and uncertainty but also allowing me to solve problems on my own. I was lucky to have been paired up with a PI that was so understanding and accommodating to his students. I will miss our talks about science and the hypothetical mechanisms that govern our research and the back and forth on outlandish theories from Shiv. I would like to thank Shiv Acharya for his help and support both inside and outside of the lab. Having a friend in the laboratory created a fun and stimulating environment. My research and table game skills improved with your help. I would like to thank Bin Lu for teaching me many of the lab techniques involved with nanopore research and for providing guidance to me even when he was on the other side of the world. Much of this work would not have been possible without the help of the undergraduates in the lab: Andre Petersen, Henry Yong, Peipei Lyu, Anderson Huang, and Chris Toh.

Chapter 1: Introduction

1.1 Introduction

Nanoparticles and lipid bilayers are essential to cell function in nature. There are many different types of cells in different shapes and sizes and even different lipid compositions[1]. Regardless of the cell variety, each has an outside barrier that protects the lumen of the cell from the extracellular space. This protective barrier, called a cell membrane, functions as a critical factor in the cell adhesions and cell-to-cell signaling and communication[2]. The inside of a cell contains organelles such as lysosomes and mitochondria[3]. These organelles are also composed of their own membrane structure. Each of these intracellular membranes provides a different purpose that allows for the organelles to function as intended. The membranes act as a barrier and as a result a pathway is needed for communication[4]. This pathway cones from permeable membrane proteins, which are selective in their nature[5]. Earlier investigations into biological membrane structures created a model called the "fluid mosaic model."[6] Biologically relevant membrane structures consist of embedded proteins and phospholipids.[7] A phospholipid consists of a lipophilic tail region and a hydrophilic head group region[8]. This lends to their amphipathic characteristic. For instance, in an oil-water interface, lipids will orient with the tail group in the organic phase and the head group facing the aqueous phase[9]. This orientation is a result of the polarizing range of hydrophobicity of the lipids[10].

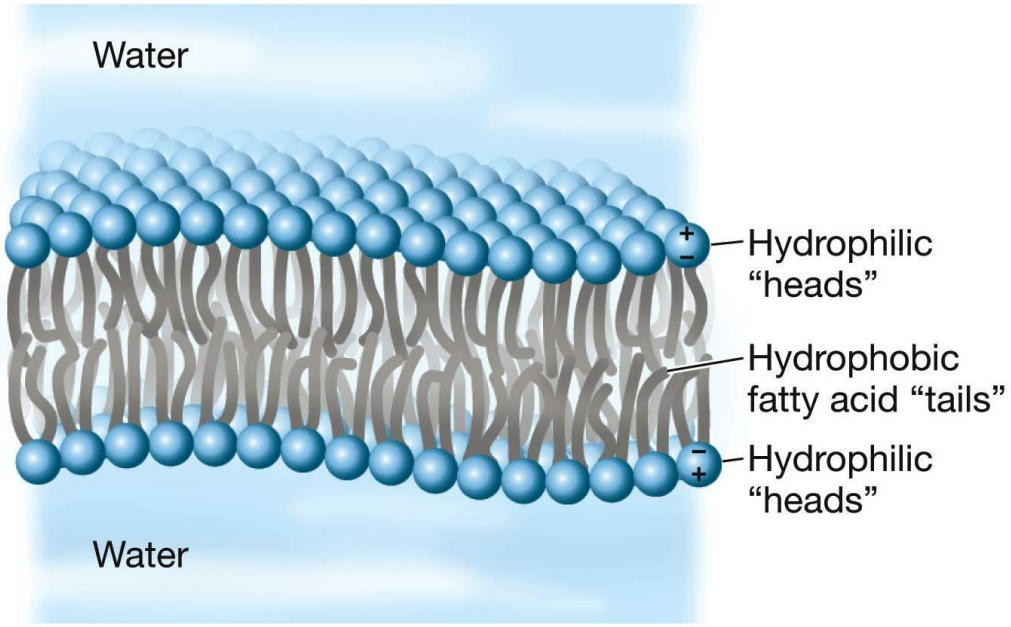

Figure 1: Lipid Bilayer Illustration: Bilayers are composed two lipid monolayers with the hydrophilic head facing out to aqueous solution and the hydrophobic tail embedded inside away from the aqueous solution. (Figure adapted from Sundava et al.[11])

There have been a variety of bilayer formation techniques over the years in an effort to have an approach that allows for a high degree of control over lipid composition and bilayer contents[12]. Approaches developed over the years include painted, folded, and droplet bilayer techniques[13].

1.2 Overview of Bilayer Creation Methods

Painted Bilayers

First introduced by Mueller and co-workers in the early 1960's, the painted bilayer technique was it was the first approach for formation of artificial lipid bilayers[14]. By spreading lipid-oil solution across a small aperture on a thin hydrophobic film, which acted

as a divider between two compartments filled with electrolyte solutions, bilayers could be reliably formed[15].

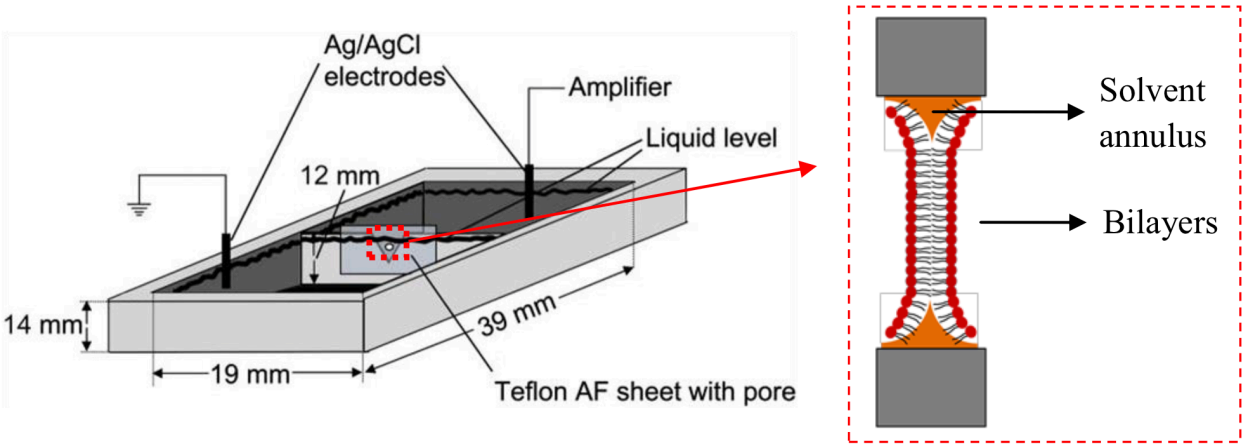

Figure 2: Painted bilayer apparatus schematic. A: Two compartments divided by Teflon® film composed of an aperture with a diameter of 50-300µm. An electrolyte solution is filled in both compartments above the aperture level. Silver chloride electrodes are connected to an amplifier and are inserted into the electrolytic solution to measure the electrical properties and characteristics of the pore. B: A cross-sectional view of the bilayer formed across the aperture. Once the bilayer has formed, a solvent annulus remains at the boundary between the bilayer and the edge of the pore. (Meyer et al.[16])

The hydrophobic film absorbed the organic solution and the lipids self-assemble into bilayers[17]. Measuring the capacitance of the bilayers can monitor bilayer formation[18]. Bilayers can be deemed fully formed once the capacitance reaches or exceeds a certain value. One of the drawbacks to this technique is the requirement of an experienced operator, with a honed technique of properly applying lipid solution across the aperture and the ability to determine if and when a bilayer has formed.

Folded Bilayers

Montal and Mueller introduced the folded bilayer technique in 1972[19]. Pre-formed lipid monolayers are brought together to form a bilayer. To form the monolayers, a small amount of hexane-lipid solution is spread over an aqueous solution. Once the hexane has evaporated, the aqueous level is raised via an addition of more solution and the monolayers are brought into contact with each other[20]. Applications of this method include studying proteins that may be sensitive to solvents[21], since this method may be considered free of solvents. Additionally, is may be possible to experiments with two different lipid compositions.

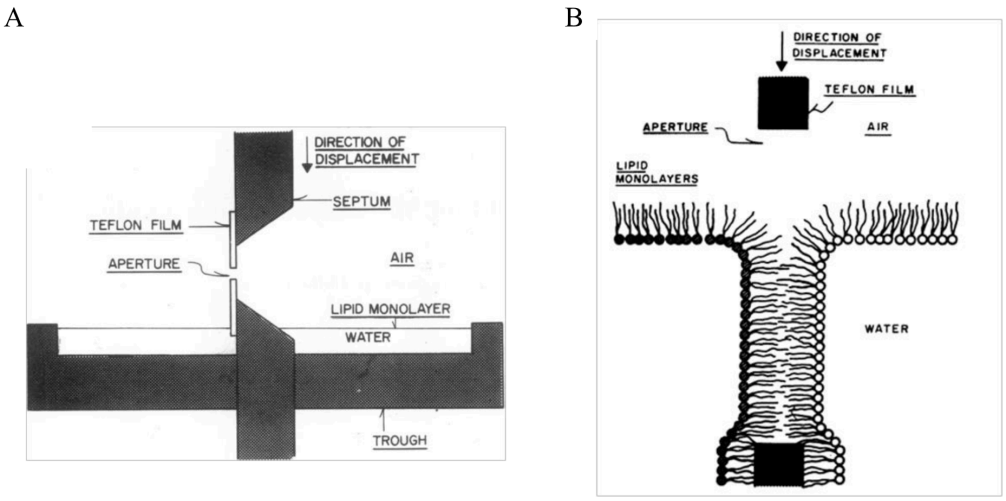

Figure 3: Folded bilayer formation. A: Bilayer formation apparatus. B: Folding two monolayers to form a bilayer. Illustrations are not to scale. (Montal and Mueller.)[19]

1.3 Droplet Bilayers

The droplet bilayer method utilizes two monolayers of phospholipids that are formed at a horizontal interface between air and two aqueous solutions[22]. As previously discussed, lipids will spontaneously orient themselves depending on the medium with which they interface. For example, in an aqueous-air interface, the head group, hydrophilic, will orient towards the aqueous phase. By raising the solution's height within the chamber over the aperture, the monolayers on each side of the partition will begin to join together at the aperture and form a bilayer. This bilayer has less solvent than in the previously discussed painted bilayer technique. Recently, a group developed a micro-fabricated chip that supported the formation of close to 100 bilayers by using a series of electrical and fluidic connections[23,24]. The same group also developed a microfluidic device that formed lipid bilayers by contacting two monolayers that self-assembled at aqueous-oil interfaces[25]. This technique is known as the method of droplet interface bilayers, first published in the mid-1960s[26]. A particular technical advantage is that the only complication in the system relied on the positioning of the droplet[27,28]. The use of micromanipulators, electrical fields, and microfluidic flows can limit this difficulty[29,30]. The ability to parallelize and automate this system lends to its main advantageous qualities[31,32].

1.4 Bilayer Measurements

Monitoring the capacitive current of the membrane serves as a way to distinguish if a bilayer has formed. A charged membrane is established by applying a triangle wave voltage of alternating a small-applied voltage. The resulting current is then measured using a computer processor. Establishing a base capacitive current before a bilayer and after a

bilayer allows for calculating the membrane size. This calculation can be done via the following equations:

$$I = C \frac{dV}{dt}$$

$$C = \epsilon_r \epsilon_0 \frac{A}{d}$$

Dielectric constant,	ϵ_0 = 8.854E-12 $F \cdot m^{-1}$
Relative statistic permittivity,	ϵ_r = 2
Bilayer thickness,	d = 5nm
Bilayer area,	A = πr^2

Rearranging the first equation to solve for C and then using this value in the second equation to solve for the area, the estimated bilayer diameter and area can be approximated. One potential drawback of this particular method is false positives of bilayer formation, as the current measured during the imposed triangle. Once the monolayers have formed so does a capacitive current; however, while the distance between monolayers in a bilayer is roughly 5nm, the distance between the two monolayers is relatively large. Once the monolayers begin to come together and join, the resulting capacitive current will grow and subsequently once the bilayer is formed the current generated by the triangle wave input voltage will begin to flatten. This result is an indication of capacitive charging and subsequently formation of the membrane. Characteristics of the capacitive current and thus bilayer formation will change based on variables of the experiment. These variables include aperture size or film thickness, solvent composition, and the lipid composition of the bilayer[33].

One way to ensure a bilayer has formed is by applying a large sudden voltage, or "zapping." This zapping breaks the bilayer with the application of a large potential. If there is no bilayer, the capacitive current will remain the same. A bilayer will break, and the resultant capacitive current will be shortened and will be easy to distinguish in the data acquisition program. Unfortunately, this bilayer formation test breaks any bilayer that had formed. This test is best used at the end of an experiment to establish the baseline size for a bilayer.

Decoding electrical measurements can initially be challenging, but once the general equations are understood deducing information can be a rather simple process. Observing the capacitive currents with this understanding makes it possible to distinguish formed bilayers from unformed bilayers without zapping the bilayers and thus ending the possibility of using the bilayers[34]. Variations in variables such as aperture size and lipid composition may require a simple recalibration of determining a bilayer capacitance threshold. A safe case with the Tecella© is assuming anything with a capacitive current above 180pA is a bilayer.

Upon establishing that a bilayer has formed, the next step is identifying interactions with the membrane. A current fluctuation threshold was established as a value deviating more than the average current value of a control well plus or minus the peak-to-peak noise level. Any fluctuation greater than this baseline value on the positive voltage portion of the trace or less than the baseline value on the negative portion of the trace was noted as a pore formation. Interactions may very in size, eventually reaching the point of a fused bilayer. A fusion refers to the two aqueous phases fusing together to allow a large flux of

current between the two chambers resulting in a pore so large the bilayer is beyond reforming. Pore formations, in general are noted as interactions. These interactions may be classified into different categories, however unless specifically noted, the notation of an interaction may be simply interpreted as a generalized pore formation event. The figure below illustrates the determination of the threshold for determination of potential pore formation, with values above the red line on the left or below the redline on the right qualifying for such a distinction.

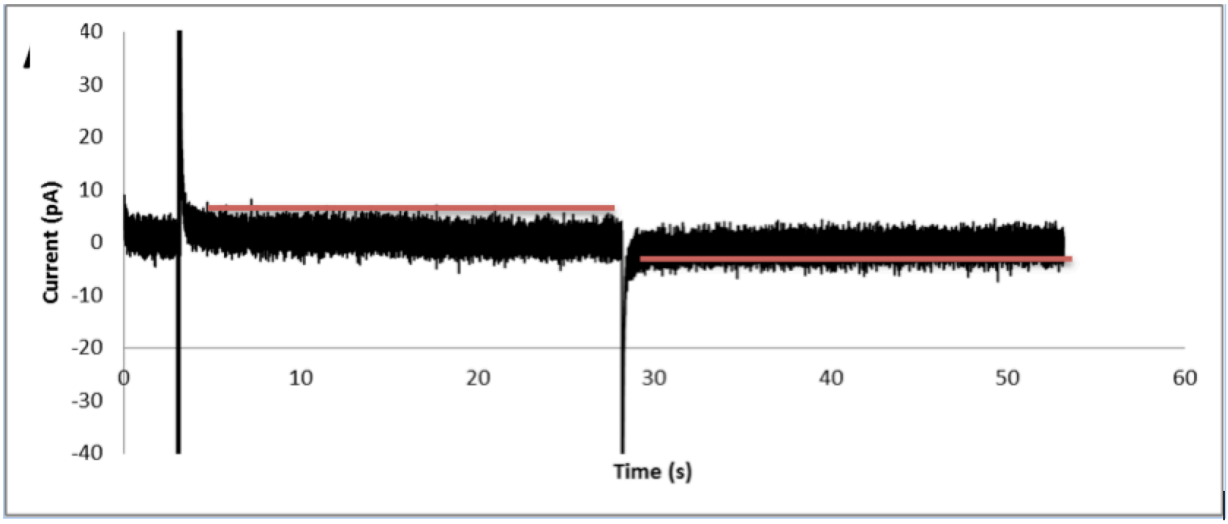

Figure 4: Example of establishing minimum current fluctuation for pore determination

Noting if an interaction takes place, the duration of the interaction, and the pore size are not the only factors that are important to consider in regards to bilayer interactions. When an interaction occurs can also be equally important. The testing protocol used for the experiments outlined in this work include positive and negative 70mV sweeps of 25 seconds each after an initial application of 0mV for 3 seconds. Conducting a number of experiments under different conditions with the same lipid bilayer composition and particle

concentration allows for investigating if nanoparticles are more or less likely, if there is a difference at all, to cause interactions and ultimately fusions with a positive or negative applied voltage.

1.5 Experimental Philosophy

The experimental philosophy of the experiments tested in this work are based on the idea of seeking to discover more information about nanoparticle interactions with lipid bilayers and possible conditions and variables that may govern these interactions. Some of the variables tested include different nanoparticles, nanoparticle concentrations, lipid compositions, ionic strengths, pH conditions, and presence or absence of serum. There is still much to learn about nanoparticle interactions with lipid bilayers and with the creation of an efficient and robust platform to create bilayers in various conditions, discussed in later sections, there was a clear opportunity to investigate a class of nanoparticles and their interactions in ways that had not been previously studied.

Chapter 2: Multichannel Horizontal Bilayer Array

2.1 Overview

One problem with conducting bilayer experiments is creating enough bilayers to have a statistically significant amount of data. Even those bilayers that do form may take hours to form under previous bilayer techniques. Low bilayer yield and inefficiency hinders research and new discoveries from being made. This problem was solved with a new technique developed out of the Schmidt lab at UCLA[35]. This method is referred to as a multichannel horizontal bilayer array for a number of reasons. The horizontal bilayer portion is reference to the fact that the aperture and thus bilayer orientation is open across the horizontal axis, difference than the typical vertical axis for painted bilayers. Secondly, the multichannel array is reference to each chip having eight wells in an array, thus supporting multiple channels. An overview of the setup is shown in the following figure.

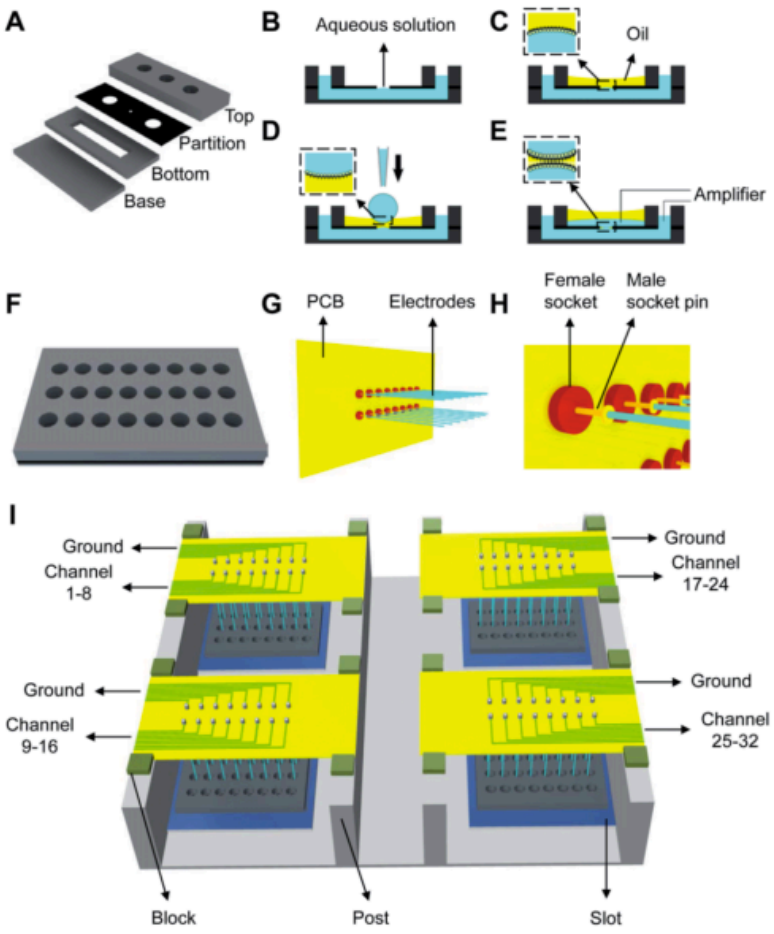

Figure 5: Illustration of multichannel horizontal bilayer array. (Figure adapted from Lu et al.[36])

The figure above illustrates the components required for the array method. Figure 5A shows expanded view of an individual channel, displaying an overview of the components of an individual chip such as Delrin® film part with a small aperture between the top acrylic piece and the bottom and base acrylic pieces. Acrylic tape, binding the partition film to the top and bottom acrylic parts, is not shown. Figure 5B through Figure 5E show illustrations of the droplet bilayer method, which is further described in Appendix A.5 Briefly, a prepared aqueous liposome solution is added to the bottom well followed by

the addition of a prepared lipid in oil solution. Following the addition of the lipid in oil solution, and after waiting for the monolayer to form, aqueous solution is added to the top and the monolayers form a bilayer. Figure 5F is an illustration of one completely manufactured bilayer chip. Figure 5G and Figure 5H are illustrations of the PCB and configurations of electrodes and their interchangeability features. Figure 5I is an overview of all of the components used in the setup. The array is composed of 32 channels, with each channel having access to a top well and two interconnected bottom wells, and each chip composing of 8 channels for a total of 4 chips. The electrodes are placed in the wells such that the active electrode is placed in the top well and the ground electrode is connected to the bottom well. Nanoparticles used in experiments discussed in this work are always added via the top well.

2.2 Materials

Acrylic materials were purchased from McMaster Carr (Santa Fe Springs, CA). Acrylics included sheets of 12”x12”x0.25” and 12”x12”x0.625” parts used for chips in the multichannel horizontal bilayer array. The figure below are examples of acrylic sheets used for assembly, highlighted in section 2.3 below.

Figure 6: Acrylic sheets used for multichannel horizontal bilayer array

Acrylic adhesive, SciGrip Acrylic Weld-on Adhesive #3, was purchased as Solter Plastics (Los Angeles, CA). The acrylic adhesive was an important component involved in the chip assembly, outlined in section 2.3 below, as it is critical to keep the wells in the array independent from one another. Delrin® film, and VHB tape were purchased from McMaster Carr (Santa Fe Springs, CA). αMEM and FBS were from Life Technologies (Camarillo, CA).

Nanoparticles were purchased from Nanocomposix, Inc (San Diego, CA) and NanoAmor, Inc (Houston, TX). The figure below shows a few examples as to the appearance of the nanoparticles in dry form.

Figure 7: Nanoparticles in raw form

Lipids and lipid composition materials used in the tests such as 1-palmitoyl-2-oleoyl-sn-glycero-3-phosphocholine (POPC), 1- palmitoyl-2-oleoyl-sn-glycero-3-phosphoethanolamine (POPE), Cholesterol (Chol), 1-palmitoyl- 2-oleoyl-sn-glycero-3-phospho-L-serine (POPS), Cerebroside (CB), and sn-(3-oleoyl-2- hydroxy)-glycerol-1-phospho-sn-1'-(3'-oleoyl-2'-hydroxy)-glycerol (BMP) were ordered from Avanti Polar Lipids, Inc (Alabaster, Alabama). Decane, methanol, and chloroform were from Sigma-Aldrich (St. Louis, MO).

2.3 Chip Fabrication, Assembly, and Prep

The Schmidt lab has created a multi-well chip array that allows for up to eight bilayers to form at a time. These chips are used in conjunction with a Tecella© amplifier, configured in lab to test up to 32 bilayers at a time. Each individual chip is composed of six individual parts: a top acrylic piece, a base acrylic piece, a ladder shaped acrylic piece, a partition made of Delrin® film, and two acrylic tape pieces which holds the chip together. The fabrication of these chips, while time consuming, allows for up to 32 bilayers to be used at once—a significant improvement in efficiency over traditional one-bilayer techniques and setups. Once the six parts are cut a chip can be assembled. Chips are typically assembled in groups of 4 to 12. The figure below shows an unassembled and assembled chip.

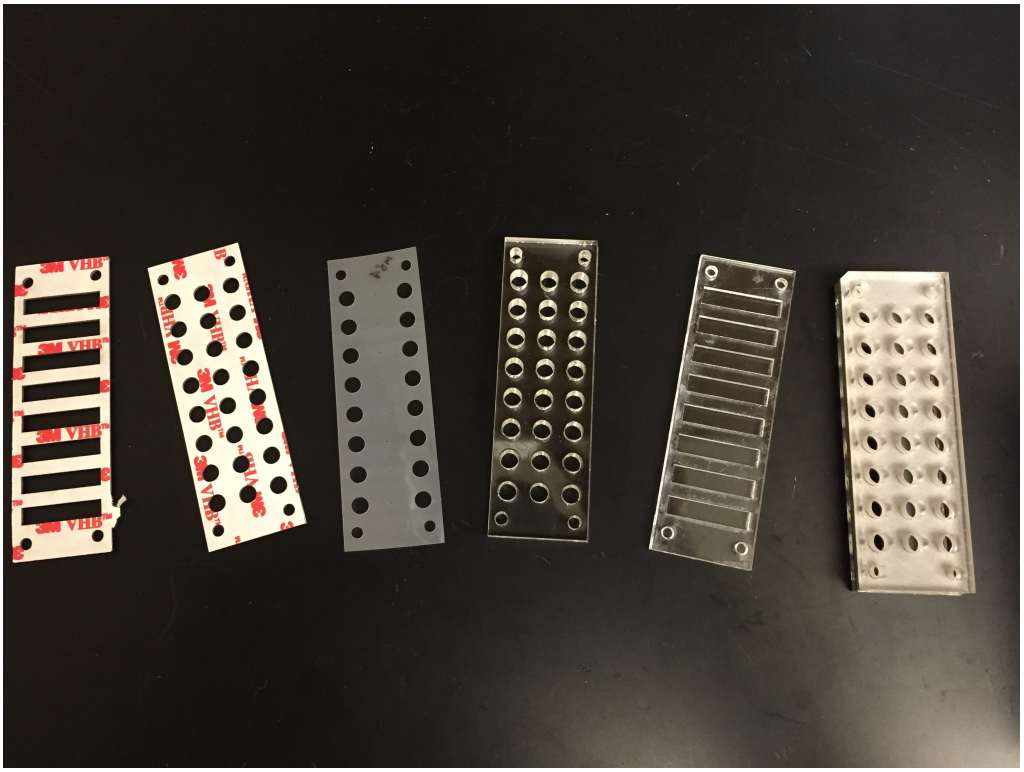

Figure 8: Chip Assembly. From left to right: bottom tape, top tape, partition, top acrylic, bottom glued acrylic, assembled chip.

Assembled chips go through a rigorous washing process to ensure that any possible contaminants are removed from the chips. This washing process, outlined in Appendix A.4 includes using decane, methanol, deionized water, pressurized air, and a desiccator.

2.4 Partition Quality Control

Each experiment condition required a specific range of partition hole sizes. At pH 4.5 with buffer on top this range was between 650 microns and 700 microns. For pH 7 and 10 with buffer on top this range was between 700 and 750 microns. For the serum

experiments, yield was best when the partition size was between 700 microns and 750 microns. Size is not the only indicator as to whether an experiment will be successful. The partition holes are supposed to be round and have smooth edges. When the partitions are irregular shapes and or have jagged edges the results can be unfavorable. The figure below exemplifies some unwanted characteristics such as jagged edges and wrong size (intended size was a diameter of 700μm).

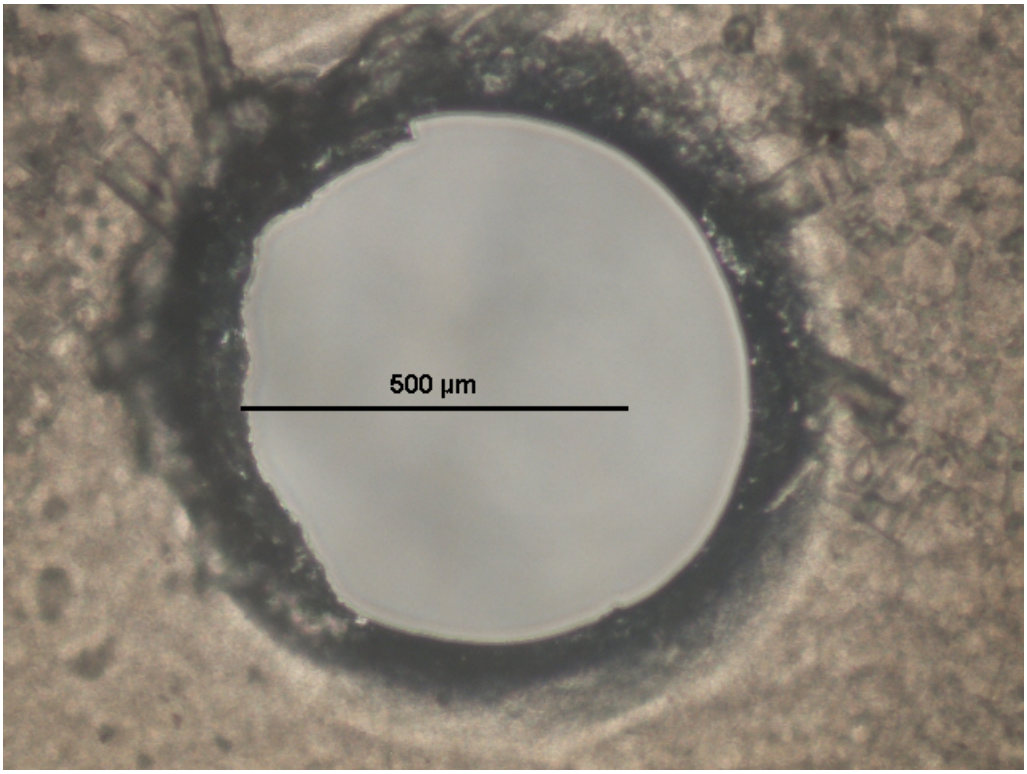

Figure 9: A partition exhibiting undesired characteristics. The left side of the shows signs of jaggedness, the hole itself is not symmetrical, and the hole size is much closer to 600μm than 700μm.

The characteristics of the partitions can be ensured with a quality control process. Partition hole sizes are chosen based on the file that the laser cutter cuts the partitions.

The file can be modified to call for the laser cutter to cut bigger or smaller hole sizes. Each partition hole can be imaged to ensure that the hole diameter and roundness are correct. A light microscope can be used obtain these images. The image settings can be manipulated to provide a high contrast between the inside and outside of each individual hole. Once an image is obtained, a program such as Matlab® can be used to analyze and quantify characteristics about the partition holes as shown in the figure below.

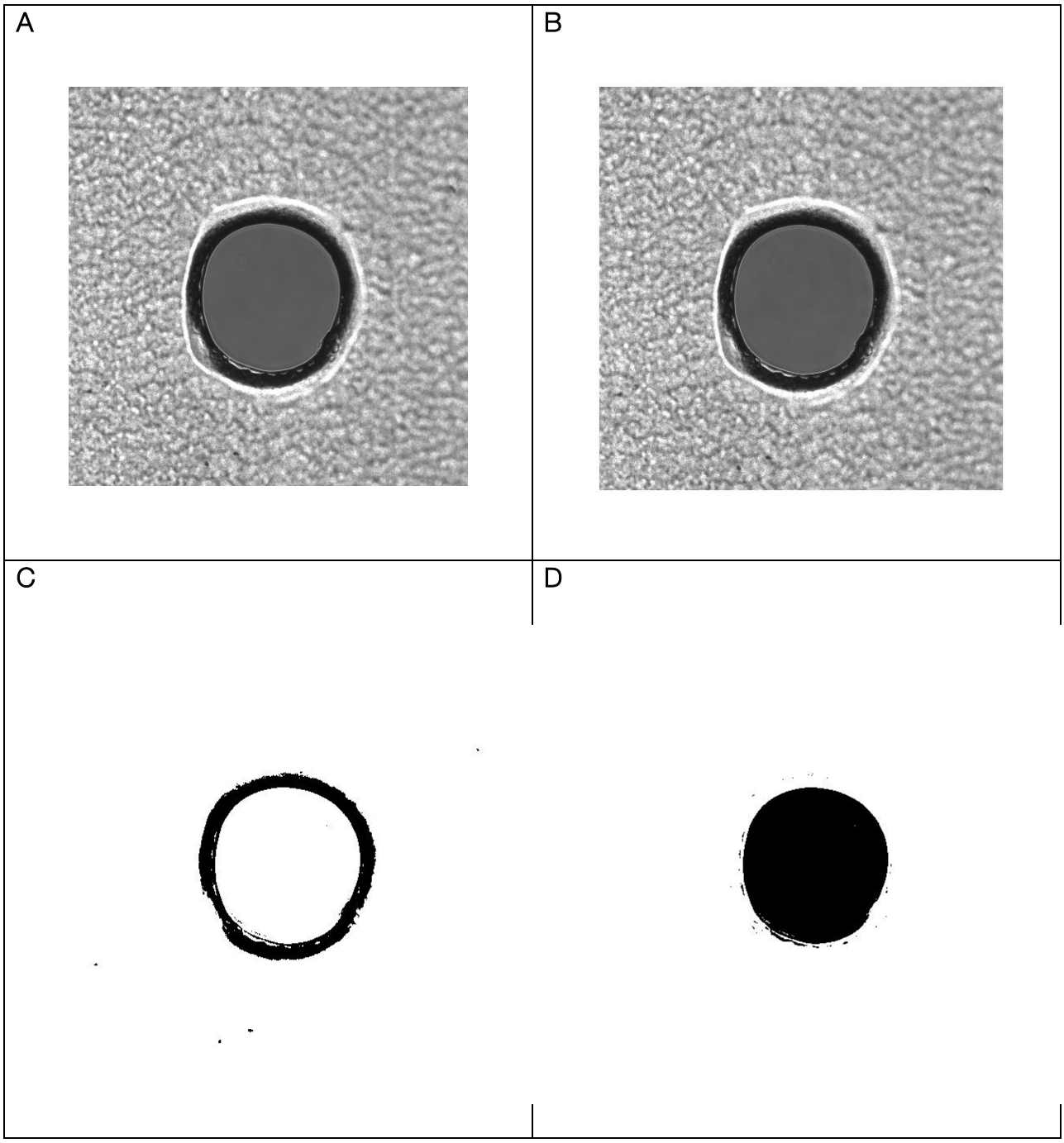

Figure 10: Partition Analysis

In the images above, the original photograph taken with the light microscope is shown in Figure 10A. This photograph is transferred to a computer with a Matlab® script

that can process the images. In Figure 10B, the original image of the partition is converted to gray scale to ease the post processing of the image. Figure 10C is the result of an image that was transformed based on threshold values of the gray scale image in Figure 10B. The outer white ring is inverted to be black. The inner and outer parts of the partition hole are converted to black. Finally, this image is process to have the inside of the ring become black, and the outer edges and beyond become white. The result is Figure 10D, which is only the inside contents of the hole and nothing else. From here the average diameter and area are readily calculated.

Since the partitions are cut in an array of 4x3, characteristics of the laser cutter can also be quantified. An image of this array is shown below.

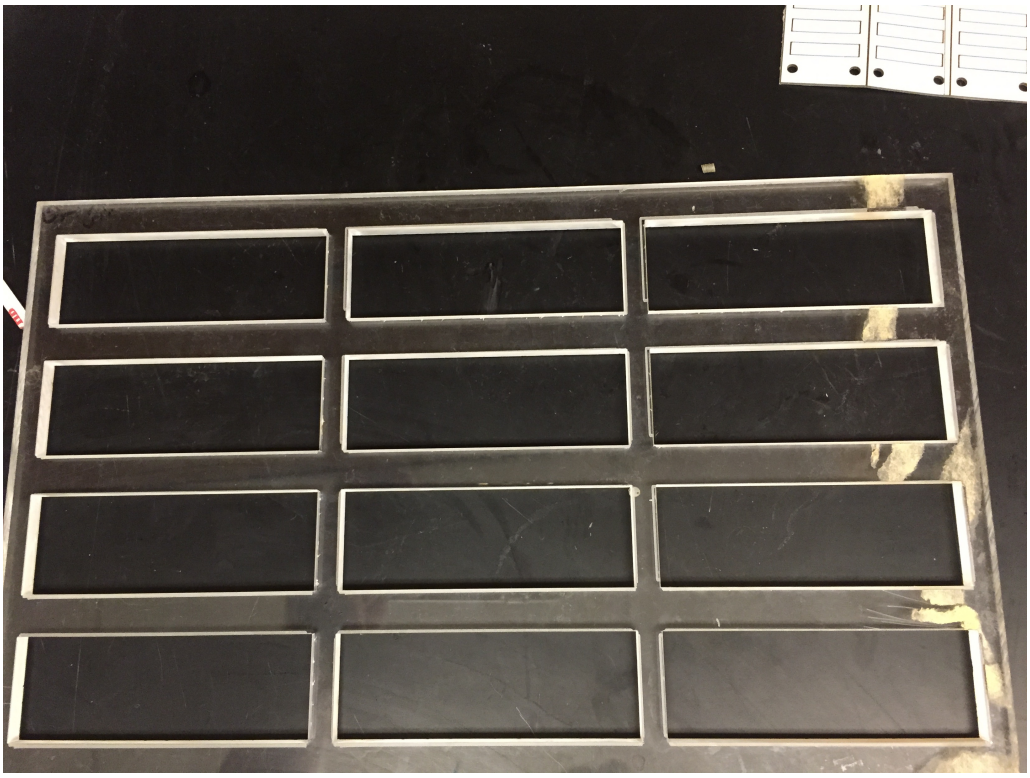

Figure 11: Laser cut partition array

It may be of note whether one area of the array is cut differently than another. For instance, if the laser cutter cuts holes accurately and at the desired size in the first column but gradually decreases in accuracy as the cutting process occurs then this is easily observed and necessary corrective action may be taken. If the holes are unified in size and shape regularity experiments using these partitions may be performed to identify which hole size is the proper size for each experimental condition.

Findings from studying this program yielded that the rightmost column cut hole size an average of 30μm larger than the leftmost column. Since this program was capable of analyzing as many images as could be taken in a sitting, the program was robust enough

to be used as a reliable tool to characterize partitions and compare them to different batches and different laser cutting setting. As the experiments changed, so did the optimum hole size and this analysis made finding the optimal hole size an easier process.

Chapter 3: Experimental Approach to Nanoparticles

3.1 Nanoparticle Overview

In the last 15 years, nanotechnology has been developing rapidly[37]. One subset of nanotechnology is nanoparticles[38]. Nanoparticles have applications on a variety of areas including drug[39] and gene delivery[40], MRI contrast enhancement[41], tissue engineering[42], fluorescent labeling[43], DNA structure probing[44], and detection of proteins[45]. Part of the breadth of applications such as tagging and labeling is due to nanoparticles existing on the same size domain as proteins[46]. Another important aspect is the fact that nanoparticles can be modified with additions of biopolymers or antibodies[47], which gives them their biocompatibility.

As previously mentioned, drug delivery is one of the applications of nanoparticles[48]. Drug delivery can be achieved by modifying nanoparticles with ligands specific to the target of interest and loading the nanoparticles with active molecules. These modified nanoparticles are transported to the target via an injection into the blood stream[49]. Once the nanoparticles reach the intended target, the receptor binds with the ligand and as a result the active molecule that was stored inside of the nanoparticle is released[50]. Nanoparticles are also used for the application of protein detection[51]. Basic cellular functions such as cell-to-cell signaling and mechanical structure are affected or triggered by proteins. Previous research has included the study of immunohistochemistry to identify protein-protein interactions by the use of nanoparticles, specifically gold nanoparticles[52].

There are numerous modifications that can be made to nanoparticles such as shapes, charges, sizes, and surface modifications, but a sample of these configurations has only recently begun investigation[53]. The development of a system and the implementation of studying various nanoparticles is imperative to furthering the field and our knowledge.

There are a number of theories as to why one metal oxide particle does not interact with bilayers while another one does interact with bilayers[54]. Most of these theories involve charge of the particles playing a role in the interactions. Electrostatic interactions may be the driving force for causing interactions to occur[55]. The lipids that make up the bilayer are charged and may change orientation if an attractive or repulsive force approaches in proximity. This change in orientation would lead to a small pore forming or a fusion of the bilayer. Another theory is that since the bilayers are horizontal in orientation and metal oxide nanoparticle do not dissolve in buffer, the force of the nanoparticles falling onto the bilayers may be strong enough for the most dense particles to fuse the bilayers.

Nanoparticles encountered in many day-to-day activities were studied. Lanthanum oxide is in exhaust-gas convectors[56], imaging and protein detection[57], as a strengthening agent[58], and as a catalytic material[59]. Cerium oxide is used as a catalyst[60], cancer therapeutics[61,62], and drug delivery[63,64]. Copper oxide is used for semiconductors[65], sensors[66,67], and detecting anti-microbial activity[68,69]. Cobalt oxide has applications in catalysis[70], sensors[71], energy storage[72], and pigments[73]. Zinc Oxide is used in sunscreens[74], facial creams[75], semiconductors[76], antibacterial activity[77], and aniti-cancer treatments[78]. Indium oxide is used in nano-electronics[79], transistors[80], photodetectors[81], and as a gas sensor[82]. Erbium oxide is used for biomedical imaging[83], display monitors[84],

and optical communication[85]. Europium oxide has applications for fluorescent labels[86] and phosphors[87]. Finally, gadolinium oxide is used as a MRI contrast agent[88,89].

3.2 Concentration Profiles

Nanoparticles were initially tested at different concentrations at pH 4.5 80mM NaCl to study their physical interaction with membranes. A concentration of 200 μg/ml was the initial starting point for testing particles. Particles that did not fuse bilayers under these conditions were repeated with higher concentrations until a majority of the bilayers fused or until it was deemed that the particle was inert in any concentration and did not interact or break bilayers. For particles that did break bilayers, the concentration was decreased until only about 50% of the bilayers fused. For several of the nanoparticles, this allowed for a concentration profile in determining the optimum concentration for which interactions occur and occur long enough for the interactions to be properly studied. These concentration profiles could be used for future experimentation to explore pore formations in a variety of conditions.

At high concentrations the nanoparticle may interact and fuse the membrane almost immediately. Unfortunately, a fast fusion provides little information about the biological mechanism. The only information to be gained is that the particle is able to quickly fuse bilayers and may have inherent qualities that allow it to interact strongly with lipid bilayers. Altering variables such as lowering the nanoparticle concentrations allow for the mechanism of nanoparticle interaction can be further investigated under conditions more that can yield more information about the interaction between the nanoparticle and the lipid bilayer. In most cases, lowering the concentration of the nanoparticles achieves

the goal of gaining a more prolonged interaction so further analysis can be performed to understand the interaction's mechanism.

3.3 Ionic Strength Profiles

A concentration for each particle was established from the pH 4.5 80mM NaCl conditions and was used for the remainder of experiments. Ionic strength profiles were tested at three different ionic strength conditions: 5mM NaCl pH 4.5, 80mM NaCl pH 4.5, and 1M NaCl pH 4.5. Different ionic strengths were tested to observe what effect, if any, ionic strength has on different nanoparticles. A high ionic strength buffer solution may screen out all of the nanoparticles, working as an inhibitor against the nanoparticles. On the other hand, a low ionic strength may prove to be very limited in screening nanoparticles. One other point in regards to a low ionic strength nanoparticle is that it may be difficult to observe small pore formations, since there would only be a limited amount of ions that would pass through the pore.

3.4 pH Profiles

Once a concentration was proven to break bilayers on a regular basis at a specific ionic strength and pH a logical experiment is to study differences between pH. When the pH is changed, there are several factors that may change. One is pKa values from lipids may be in the range between pH values. For example, an amine group in a lipid with a pKa value of 9.0 is likely deprotonated at a pH of 10. Changes in protonation effect the electrostatic interactions between a lipid and a nanoparticle. The values of the pKa's for

the lipids used in the test are readily available, however it is possible that the metal oxide nanoparticles also have a pI. Future experiments analyzing the zeta potential of these metal oxide nanoparticles could provide information on whether the charge of the nanoparticles is having a large effect in different pH ranges. Three different pH values were tested in the following conditions: pH 4.5 80mM NaCl, pH 7.0 80mM NaCl, and pH 10.0 80mM NaCl. In nature, bilayers may be found in each of these pH ranges. Understanding the interaction nanoparticles have in each of these conditions could be valuable information for fusing cell membranes or creating pores in membranes to deliver particles.

3.5 Serum Experiments

Serum experiments were conducted to further test the platforms analogousness to a real cell. A cell has a bilayer with a salt concentration on one side and a serum solution on the other side. In many physiological conditions, a cellular plasma membrane is in an environment with a significant concentration of serum proteins[90]. This environment and potential effect was investigated by introducing serum to one side of the lipid bilayer. In stead of buffer solution on both sides, one side had a buffer solution, pH 7.0 150mM NaCl, and one side had a medium composed of 89% αMEM, 10% Fetal Bovine Serum (FBS), and 1% Streptomycin.

Serum solution was particularly challenging to work with because the bilayers were generally difficult to form and were very sensitive to the bottom well volume and aperture size and lipid composition. Hole size was adjusted and Neutral Super Combo was used to increase stability of the bilayers. In spite of the low bilayer yield, the effect of serum solution

on the interaction and fusion rates of metal oxide nanoparticles can be observed. This setup allowed for testing the effect serum has on these nanoparticle interactions.

3.6 Example Results

Before delving into the nanoparticle data, it may be best to observe a sample set of data and results. An example of a trace containing pore formation is shown in the figure below.

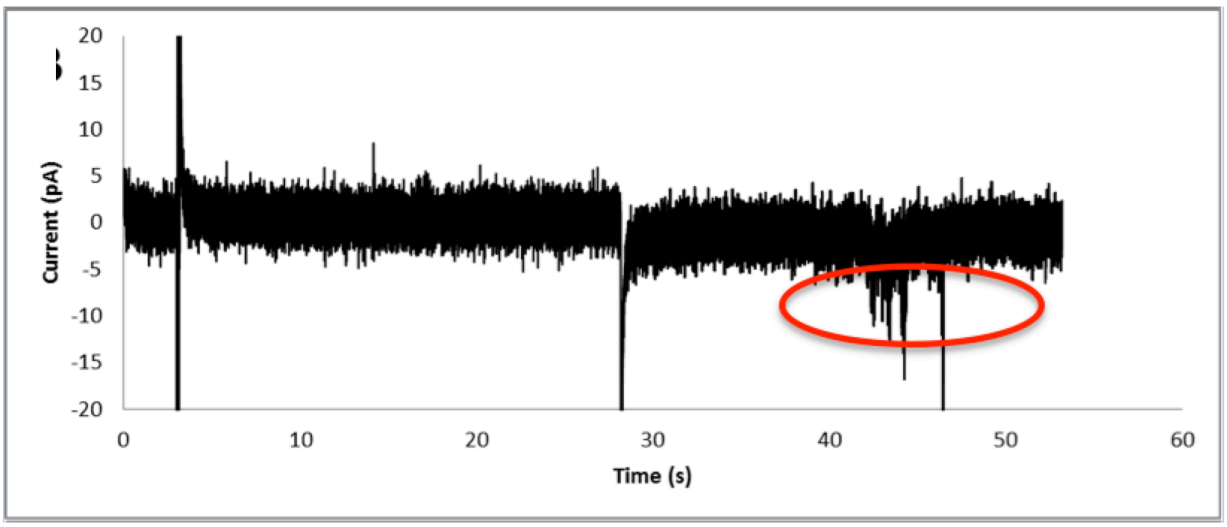

Figure 12: Example of simple pore formations/interactions highlighted in red. Changes in current are small spikes much larger than the adjacent background noise. Spikes are short in duration.

The previous figure displayed pore formations that were easy to identify compared to the baseline noise without any interactions. These pore formations may also arrive in clearly defined steps. In nature these step changes and transient pore formations may be

common due to an analytes ability to make a repeatable pore size in the membrane. An example of one of these transient pore formations is shown below.

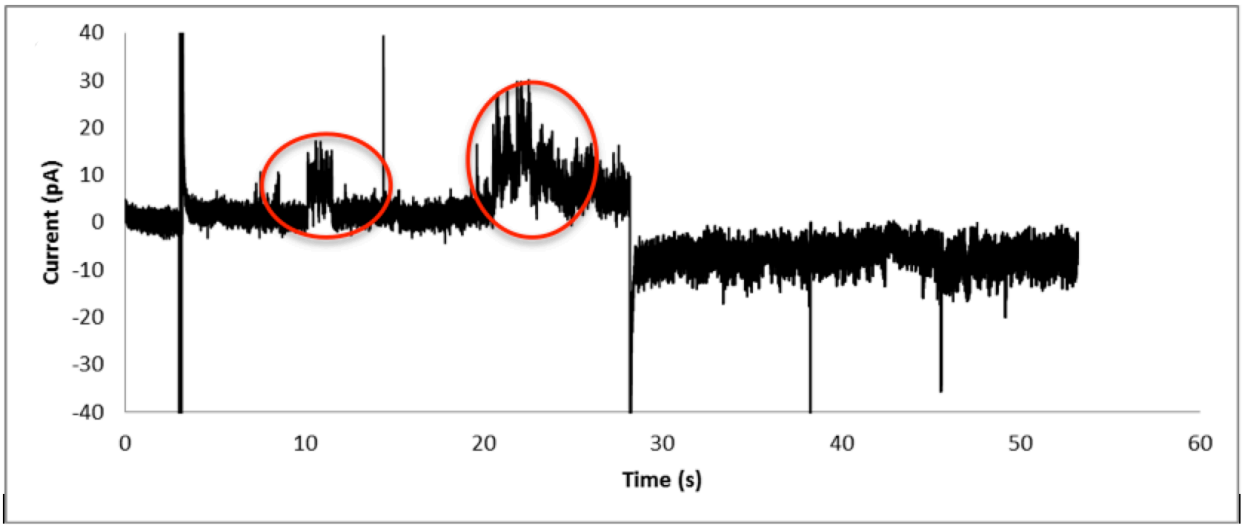

Figure 13: Example of transient pore formations highlighted in red. Changes in current are small to large spikes larger magnitude in comparison adjacent background noise. Transient pore spikes are longer in duration and may be a relatively constant current during formation.

As previously discussed, the time when the pore formations occur is also an important aspect. If the particle's interactions are only occurring or mostly occurring on either the positive or negative applied voltage sweeps then the particle most likely has some relation to voltage dependency. The figure below illustrates an example of a voltage dependent particle.

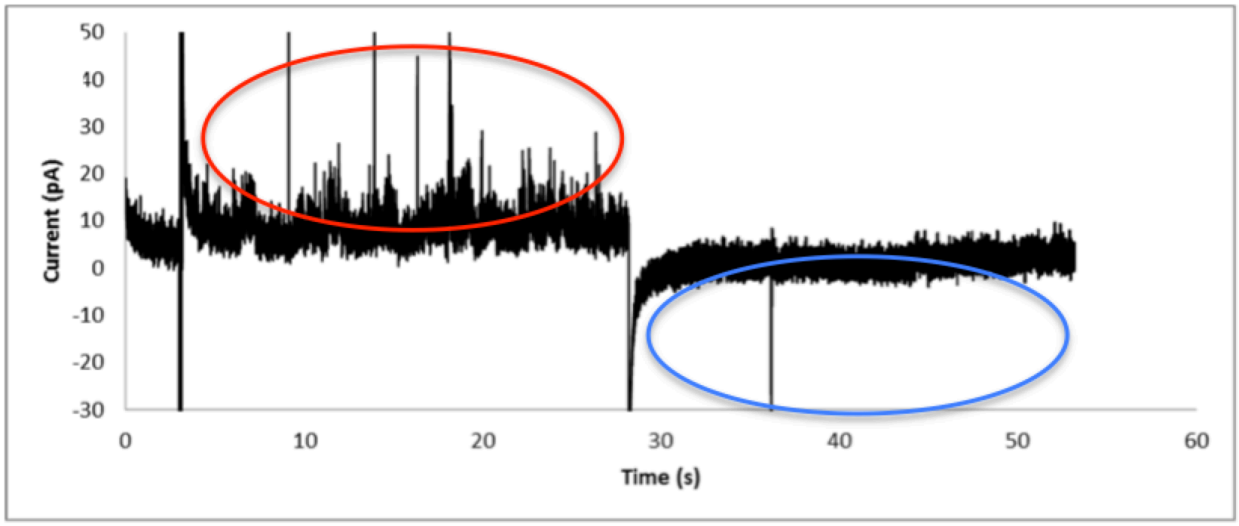

Figure 14: Example of voltage dependency. Current fluctuations, encapsulated in red are present on the left half of the figure, the positive applied voltage section. A lack of current fluctuations or pore formations, shown in blue, on the right half of the figure, the negative applied voltage portion of experimental protocol.

Eventually most interactions build up to a fusion event. As previously discussed, a fusion event is an event where a large flux if current is able to pass through the bilayer. The hole that is formed is so massive that membrane is beyond repair. An example of a fusion event is shown in the figure below.

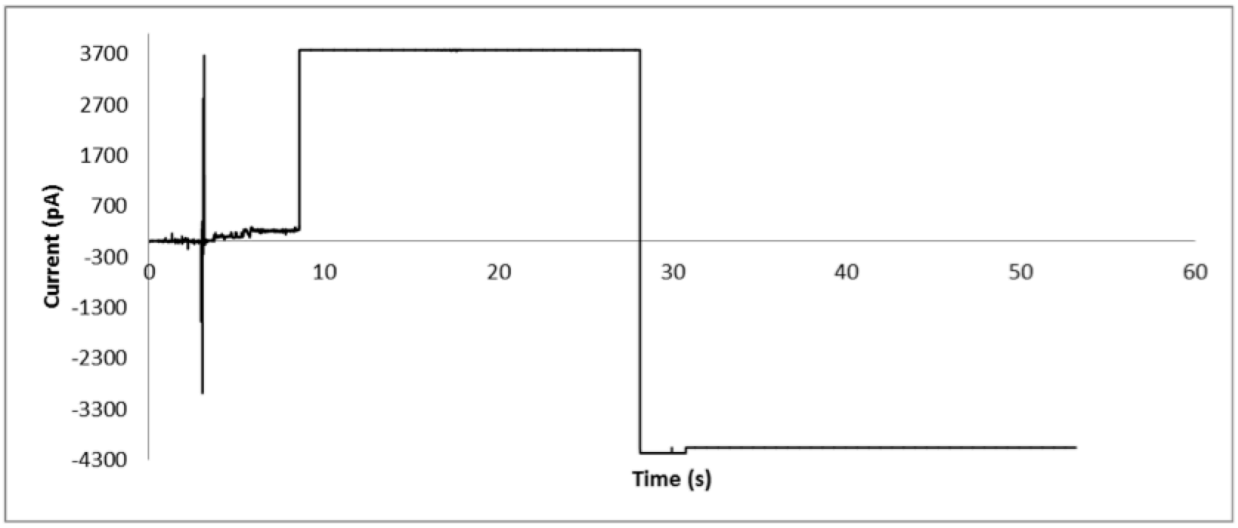

Figure 15: Example of a fusion event

These are the main characteristics that may be of importance to the success of the project. The results in the sections following will discuss and identify these characteristics.

Chapter 4: Nanoparticle Results & Discussion

4.1 Nanoparticle Results Overview

As previously discussed, each nanoparticle was screened at various concentrations at pH 4.5 in 80mM NaCl 5mM Tris-HCl until the nanoparticle concentration reached a point at which the nanoparticle exhibited interactions with the bilayer but did not immediately fuse the bilayer. Each of these concentrations and results are detailed in each nanoparticle's subchapter below. Once the desired concentration was found, tests of varying ionic strength, pH, and serum conditions were tested. A summary of each can be found in the figures below.

Ionic strength was tested in pH 4.5 buffer solutions of 5mM, 80mM, and 1M NaCl. A summary of these results can be observed in the figure below.

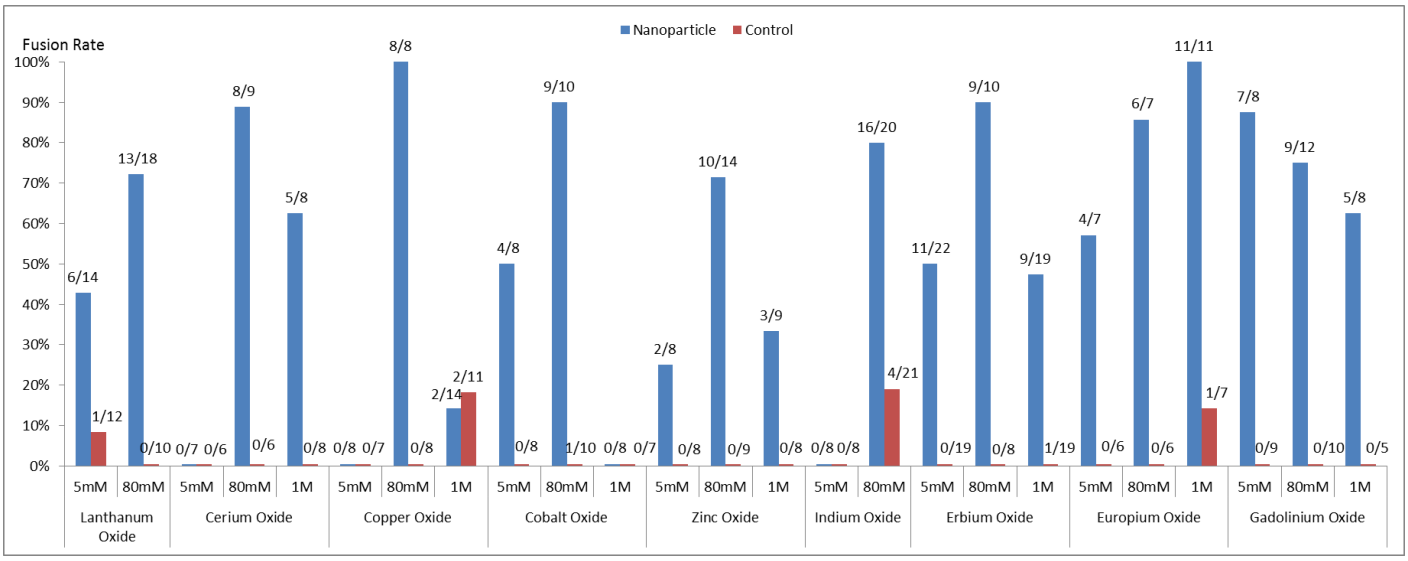

Figure 16: Ionic Strength Experiment Data Summary

Lanthanum oxide, cerium oxide, copper oxide, cobalt oxide, zinc oxide, indium oxide, and erbium oxide each had more fusions at 80mM NaCl than at 5mM NaCl and 1M NaCl. This may suggest that 80mM was the optimum salt concentration for interactions to occur with the bilayer. 5mM may have been too low for enough ions to flow through any pore that could have been potentially formed by the nanoparticles and 1M NaCl may have screened out the charge, preventing the nanoparticles from interacting with the bilayer and forming a pore. Europium oxide's results are particularly interesting. This was the only the only particle to fuse the most bilayers in this the high salt condition. Preliminary lab results using a zetasizer in the Segura lab have given values between ±6mV to ±15mV suggesting coagulation and instability. More testing with the zetasizer will need to be conducted to confirm colloidal stability to literature values.

The effect of pH on nanoparticle activity was also studied, a pH of 4.5 and 7.0 in 80mM NaCl solution were used to investigate this area of interest. A summary of this data can be found in the figure below.

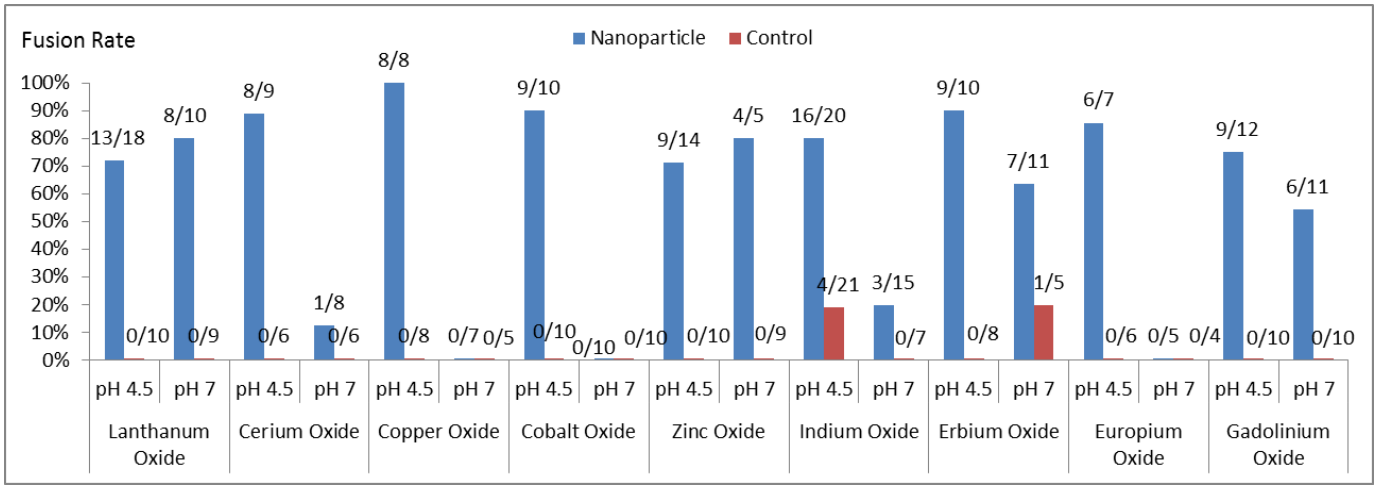

Figure 17: pH Experiment Data Summary

Cerium oxide, copper oxide, cobalt oxide, indium oxide, and europium oxide exhibited similar results. These nanoparticle had a significant drop in fusion rates from pH 4.5 to 7.0. This may be related to a potential isoelectric point, pI, at which the nanoparticle may be electrically neutral, possibly inhibiting their ability to fuse bilayers. Lanthanum oxide, zinc oxide, erbium oxide, and gadolinium oxide do not exhibit a drop off of fusion rates at the higher pH value, perhaps not yet encountering their potential isoelectric point. The lipids used in the experiments have pKa values as well, yet were relatively stable when bilayers formed. Bilayer yield was significantly lower in the pH 7.0 condition, however this was partially mitigated by optimizing the partition hole size, as previously explained.

The last comparison experiments were testing the nanoparticles in the presence or absence of serum solution. A summary of this data can be found in the figure below.

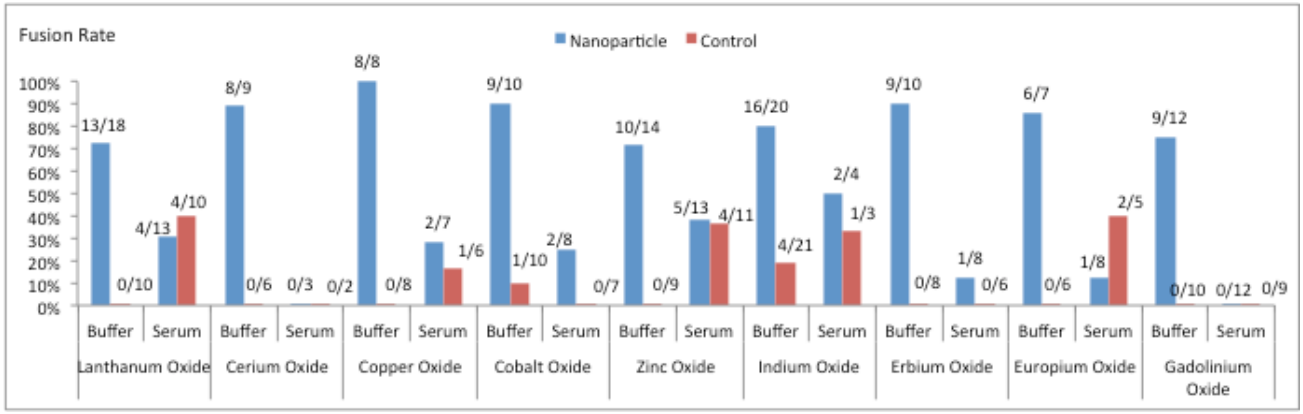

Figure 18: Serum Experiment Data Summary

In the case of serum's presence or absence, every nanoparticle tested had fewer fusions in the buffer solution than in the serum solution. This suggests that the serum solution has a strong effect on inhibiting the nanoparticle from fusing a lipid bilayer. More data for serum experiments may need to be collected to investigate this interaction relationship. Many of the serum solution experiments have a low number of tests due to the difficulty of forming stable bilayers in the serum presence condition.

The remainder of this chapter includes subchapters with details for each particle. These details include fusion tables for concentration, ionic strength, pH, and serum presence in addition to traces of each particle for typical interactions and fusions.

4.2 Lanthanum Oxide (La_2O_3)

Lanthanum oxide was initially screened at concentrations of 500 µg/ml and 100 µg/ml. As the table below shows, lanthanum oxide exhibited strong signs of activity even at small amounts.

Table 1: Lanthanum Oxide Initial Fusion Rate Experiments

La_2O_3 pH 4.5 80mM NaCl 5mM Tris-HCl		
	Bilayer Fusion Rate	
Concentration	Control Wells	Experimental Wells
500 µg/ml	0/3	3/5
100 µg/ml	0/10	13/18

Even at lower concentrations, such as 100 µg/ml lanthanum oxide proved to break the bilayers at a high percentage, however the time to fuse was longer than at 500 µg/ml and allowed for more observations of pore formation. 100 µg/ml was the particle concentration used for the remainder of experiments.

The figure below displays a typical control bilayer in a test with lanthanum oxide, a bilayer with interactions typical for lanthanum oxide, and a typical fusion event for lanthanum oxide.

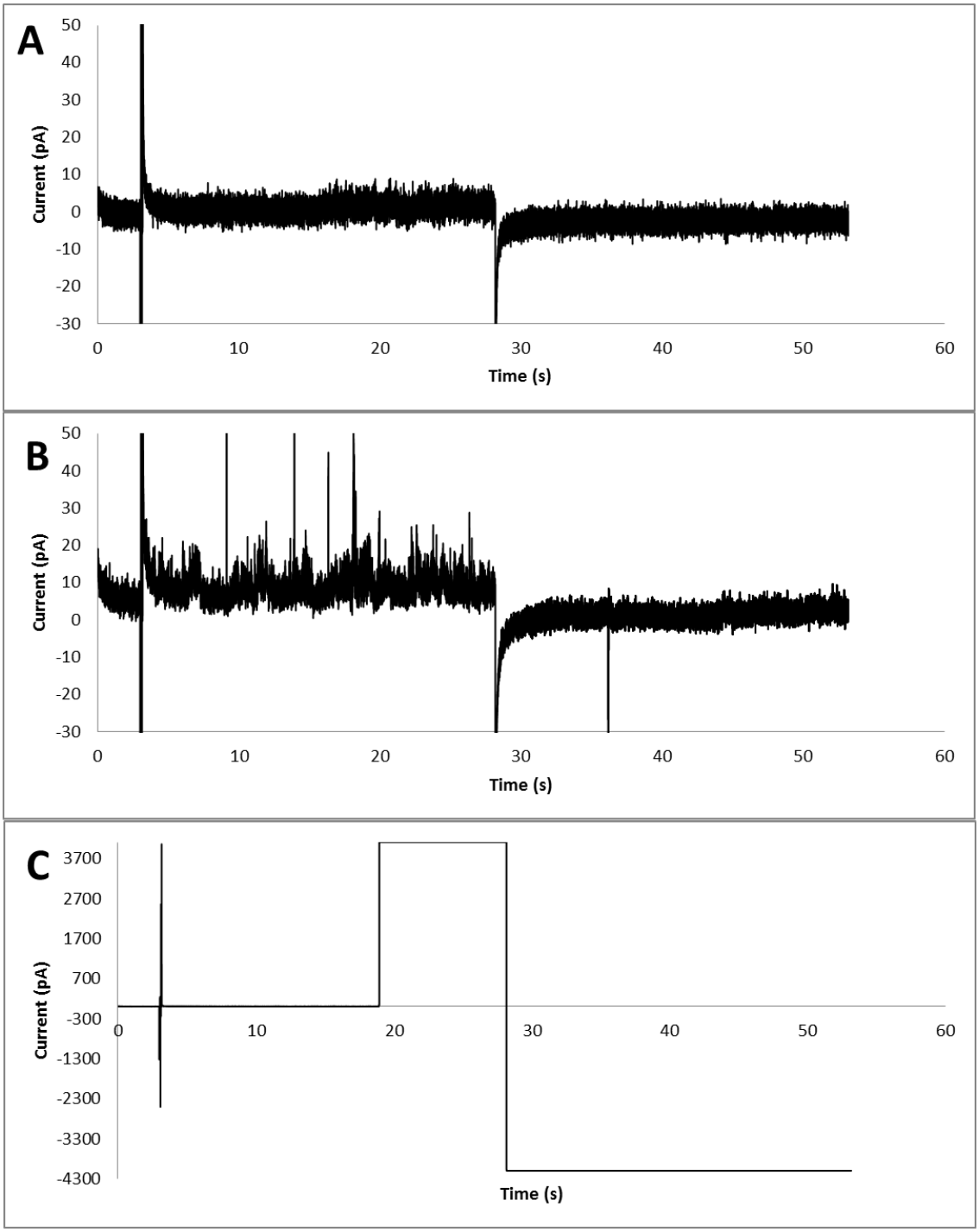

Figure 19: Lanthanum Oxide (100 µg/ml): A: Typical trace of an experimental well with particle added. B: Typical trace of a control well with buffer added. C: Typical trace of an interaction event in an experimental well after particle has been added. D: Typical trace of a fusion event of an experimental well after particle has been added.

The figure above shows that there may be strong voltage dependence for this nanoparticle. Pore formation is significant on the positive applied voltage portion of the testing protocol but minimal on the negative portion. Current fluctuations reached as large as 40pA. The fusion also occurred on the positive side. This may be of interest in future analysis of pore formation.

Ionic strength was the next test for lanthanum oxide. The table below displays the fusion rates for each condition.

Table 2: Lanthanum Oxide Ionic Strength Experimental Fusion Rates

La_2O_3 (100 µg/ml)		
	Bilayer Fusion Rate	
Buffer	Control Wells	Experimental Wells
pH 4.5 5mM NaCl 5mM Tris-HCl	1/12	6/14
pH 4.5 80mM NaCl 5mM Tris-HCl	0/10	13/18

The results of the ionic strength test showed that there wasn't much of an affect from high to low ionic strengths. Lanthanum oxide exhibited the most fusions at 80mM NaCl, typical of most nanoparticles investigated in this study. The control bilayers were not reactive in terms of fusions and had little to no interactions.

pH was the next test for lanthanum oxide. The following table below shows the changes exhibited by the lanthanum oxide at pH 4.5 and 7.0.

Table 3: Lanthanum Oxide pH Range Experimental Fusion Rates

La_2O_3 (100 µg/ml)		
	Bilayer Fusion Rate	
Buffer	Control Wells	Experimental Wells
pH 4.5 80mM NaCl 5mM Tris-HCl	0/10	13/18
pH 7.0 80mM NaCl 5mM HEPES	0/9	8/10

Unlike some nanoparticles tested, lanthanum oxide's ability to break bilayers was not turned off at pH 7.0. There wasn't much of an affect from an acidic pH of 4.5 to a neutral pH of 7.0. The control bilayers were not reactive in terms of fusions and had little to no interactions.

Serum experimental results were the same as other particles, where the presence of serum resulted in a lower fusion rate. The following table is results from these experimental conditions. Control wells were as unstable as the experimental wells, suggesting that even the wells that fused in the experimental wells may not have been necessarily due to the nanoparticle alone.

Table 4: Lanthanum Oxide Serum Experimental Fusion Rates

La_2O_3 (100 µg/ml)		
	Bilayer Fusion Rate	
Condition	Control Wells	Experimental Wells
Buffer only (pH 4.5 80mM NaCl 5mM Tris-HCl)	0/10	13/18
Serum (with pH 7.0 80mM NaCl 5mM HEPES buffer)	4/10	4/13

4.3 Cerium Oxide (CeO_2)

Cerium oxide was tested at 500 µg/ml and 200 µg/ml at pH 4.5 with 80mM NaCl 5mM Tris-HCl buffer solution. As the table below shows, cerium oxide exhibited strong signs of activity even at small amounts.

Table 5: Cerium Oxide Initial Fusion Rate Experiments

CeO_2 pH 4.5 80mM NaCl 5mM Tris-HCl		
	Bilayer Fusion Rate	
Concentration	Control Wells	Experimental Wells
500 µg/ml	0/6	8/8
200 µg/ml	0/6	8/9

Cerium oxide broke bilayers the low concentration of 200 µg/ml at a high percentage but also allowed for more interactions to occur before fusing in comparison to

the 500 µg/ml concentration. The figures below display a control bilayer tested along side cerium oxide, an typical cerium oxide interaction or pore formation, and a fusion event.

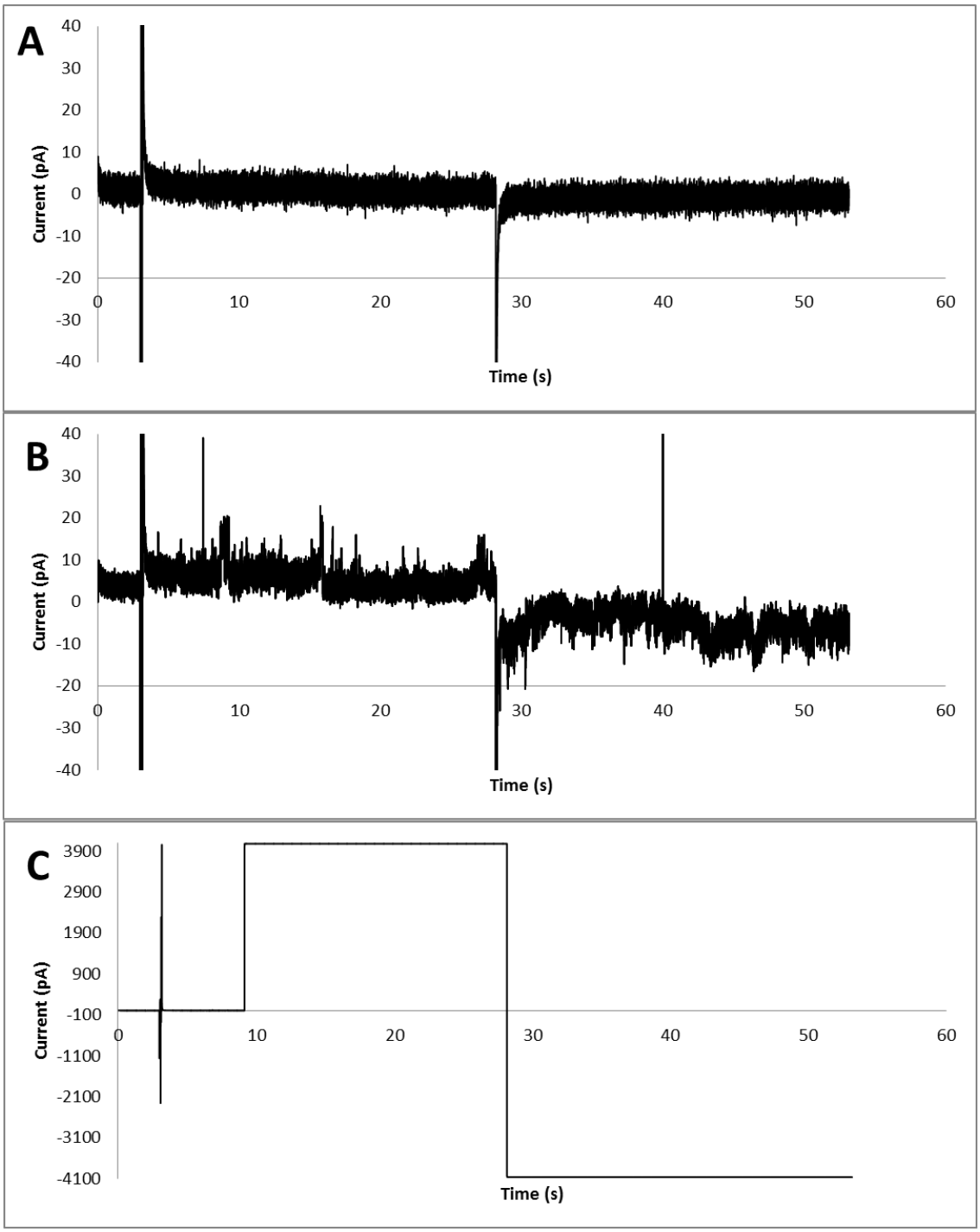

Figure 20: Cerium Oxide (200 µg/ml): A: Typical trace of an experimental well with particle added. B: Typical trace of a control well with buffer added. C: Typical trace of an interaction event in an experimental well after particle has been added. D: Typical trace of a fusion event of an experimental well after particle has been added.

The figure above shows that cerium oxide was equally reactive with both a positive applied voltage and a negative applied voltage. Pore formations occurred with current fluctuations of 10-20pA.

Different ionic strengths were tested with buffer solution of pH 4.5 NaCl at 5mM. 80mM, and 1M. The table below displays the fusion rates for cerium oxide.

Table 6: Cerium Oxide Ionic Strength Experimental Fusion Rates

CeO_2 (200 µg/ml)		
	Bilayer Fusion Rate	
Buffer	Control Wells	Experimental Wells
pH 4.5 5mM NaCl 5mM Tris-HCl	0/6	0/7
pH 4.5 80mM NaCl 5mM Tris-HCl	0/6	8/9
pH 4.5 1M NaCl 5mM Tris-HCl	0/8	5/8

The results of the ionic strength test showed that there was a significant difference between the 5mM experiment and the 80mM and 1M experiments. As previously discussed, many of the nanoparticles had these results. The control bilayers were not reactive in terms of fusions and had little to no interactions.

pH was next tested at 4.5 and pH 7.0 at 80mM NaCl and tests with the experimental particles were conducted alongside control particles to ensure interactions and fusions were related to the particles. The following results in the table below show the changes exhibited by the particle in the different conditions.

Table 7: Cerium Oxide pH Range Experimental Fusion Rates

CeO_2 (200 µg/ml)		
	Bilayer Fusion Rate	
Buffer	Control Wells	Experimental Wells
pH 4.5 80mM NaCl 5mM Tris-HCl	0/6	8/9
pH 7.0 80mM NaCl 5mM HEPES	0/6	1/8

The results of the different pH value tests, 4.5 and 7.0, yielded a significant difference. The control bilayers were not reactive in terms of fusions and had little to know interactions. Perhaps this phenomenon can be attributed to a potential change in electrostatics.

The particle was also tested in a serum environment with the previously described FBS/alpha-MEM/streptomycin. The following table is results from these experimental conditions.

Table 8: Cerium Oxide Serum Experimental Fusion Rates

CeO_2 (200 µg/ml)		
	Bilayer Fusion Rate	
Condition	Control Wells	Experimental Wells
Buffer only (pH 4.5 80mM NaCl 5mM Tris-HCl)	0/6	8/9
Serum (with pH 7.0 80mM NaCl 5mM HEPES buffer)	0/2	0/3

The results of the serum vs. no serum tests, with pH 4.5 80mM NaCl 5mM HEPES buffer, yielded a significant difference. More tests may need to be conducted since the number of bilayers tested is low, a result of the difficulty of forming bilayers in serum.

4.4 Copper Oxide (CuO)

Copper oxide was initially screened at 500 µg/ml and 100 µg/ml. Copper oxide exhibited many interactions and fusions even at small amounts, highlighted in the table below.

Table 9: Copper Oxide Initial Fusion Rate Experiments

CuO pH 4.5 80mM NaCl 5mM Tris-HCl		
	Bilayer Fusion Rate	
Concentration	Control Wells	Experimental Wells
500 µg/ml	0/8	10/11
100 µg/ml	0/8	8/8

At 100 µg/ml, this particle proved to break the bilayers at a high percentage, yet also provided details of pore formation before fusion occurred. The figure below shows a control bilayer that was tested alongside copper oxide, a bilayer exposed to copper oxide exhibiting pore formations, and a fusion event for this particular particle.

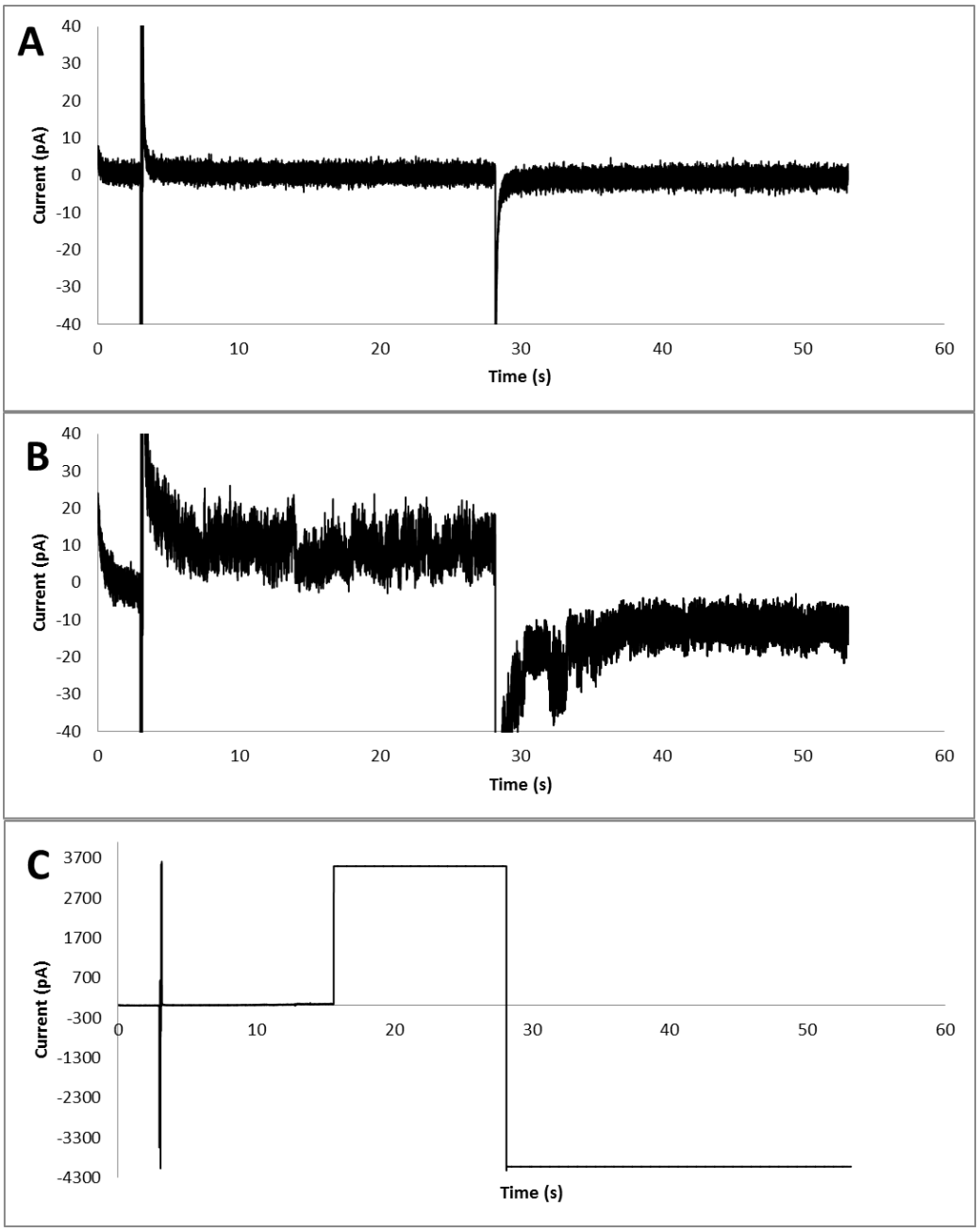

Figure 21: Copper Oxide (100µg/ml): A: Typical trace of an experimental well with particle added. B: Typical trace of a control well with buffer added. C: Typical trace of an interaction event in an experimental well after particle has been added. D: Typical trace of a fusion event of an experimental well after particle has been added.

The figure above shows current fluctuations of 15-20pA and a lack of voltage dependence as a pore formation was occurring in both the positive and negative portions of the experiment.

For the ionic strength experiments, the table below displays the fusion rates for each test for this nanoparticle.

Table 10: Copper Oxide Ionic Strength Experimental Fusion Rates

CuO (100 µg/ml)		
	Bilayer Fusion Rate	
Buffer	Control Wells	Experimental Wells
pH 4.5 5mM NaCl 5mM Tris-HCl	0/7	0/8
pH 4.5 80mM NaCl 5mM Tris-HCl	0/8	8/8
pH 4.5 1M NaCl 5mM Tris-HCl	2/11	2/14

The results of the ionic strength test showed that 80mM was the optimal condition, as it was for most of the nanoparticles tested. Possible explanations for this were previously discussed.

IpH 4.5 and pH 7.0 test with the experimental particles were conducted alongside control particles to ensure interactions and fusions were related to the particles. The following results in the table below show the changes exhibited by the particle in the different conditions.

Table 11: Copper Oxide pH Range Experimental Fusion Rates

CuO (100 µg/ml)		
	Bilayer Fusion Rate	
Buffer	Control Wells	Experimental Wells
pH 4.5 80mM NaCl 5mM Tris-HCl	0/8	8/8
pH 7.0 80mM NaCl 5mM HEPES	0/5	0/7

There was a strong affect from an acidic pH of 4.5 to a neutral pH of 7.0, almost as if the nanoparticles fusing power was turned off as the pH was increased. The control bilayers were not reactive in terms of fusions and had little to know interactions. Perhaps this phenomenon can be attributed to the nanoparticles potential change in electrostatics.

The following table has results from the serum experiments.

Table 12: Copper Oxide Serum Experimental Fusion Rates

CuO (100 µg/ml)		
	Bilayer Fusion Rate	
Condition	Control Wells	Experimental Wells
Buffer only (pH 4.5 80mM NaCl 5mM Tris-HCl)	0/8	8/8
Serum (with pH 7.0 80mM NaCl 5mM HEPES buffer)	1/6	2/7

There was a significant difference from the experiment with buffer only and the experiment with serum on one side of the bilayer. This means that any potential screening

resulting from the serum solution may have been occurring and resulted in the particle being unable to disrupt the bilayer. The control bilayers were more reactive in terms of fusions in comparison to previous test, likely due to instability caused by the serum, yet even with a potential extra amount of fusions for the experimental wells based simply on instability, the experimental wells in the serum experiments yielded significantly fewer fused bilayers.

4.5 Cobalt Oxide (Co_3O_4)

Cobalt oxide was studied at 500 µg/ml and 100 µg/ml. The table below shows the fusion results for these two concentrations.

Table 13: Cobalt Oxide Initial Fusion Rate Experiments

Co_3O_4 pH 4.5 80mM NaCl 5mM Tris-HCl		
	Bilayer Fusion Rate	
Concentration	Control Wells	Experimental Wells
500 µg/ml	1/10	9/10
100 µg/ml	1/10	2/10

At the low concentration, 100 µg/ml, this particle was not able to fuse bilayers at a high rate like the other particles. The figure below is of a control trace that was tested at the same time as the experimental wells, an experimental well with interactions, and a fusion event.

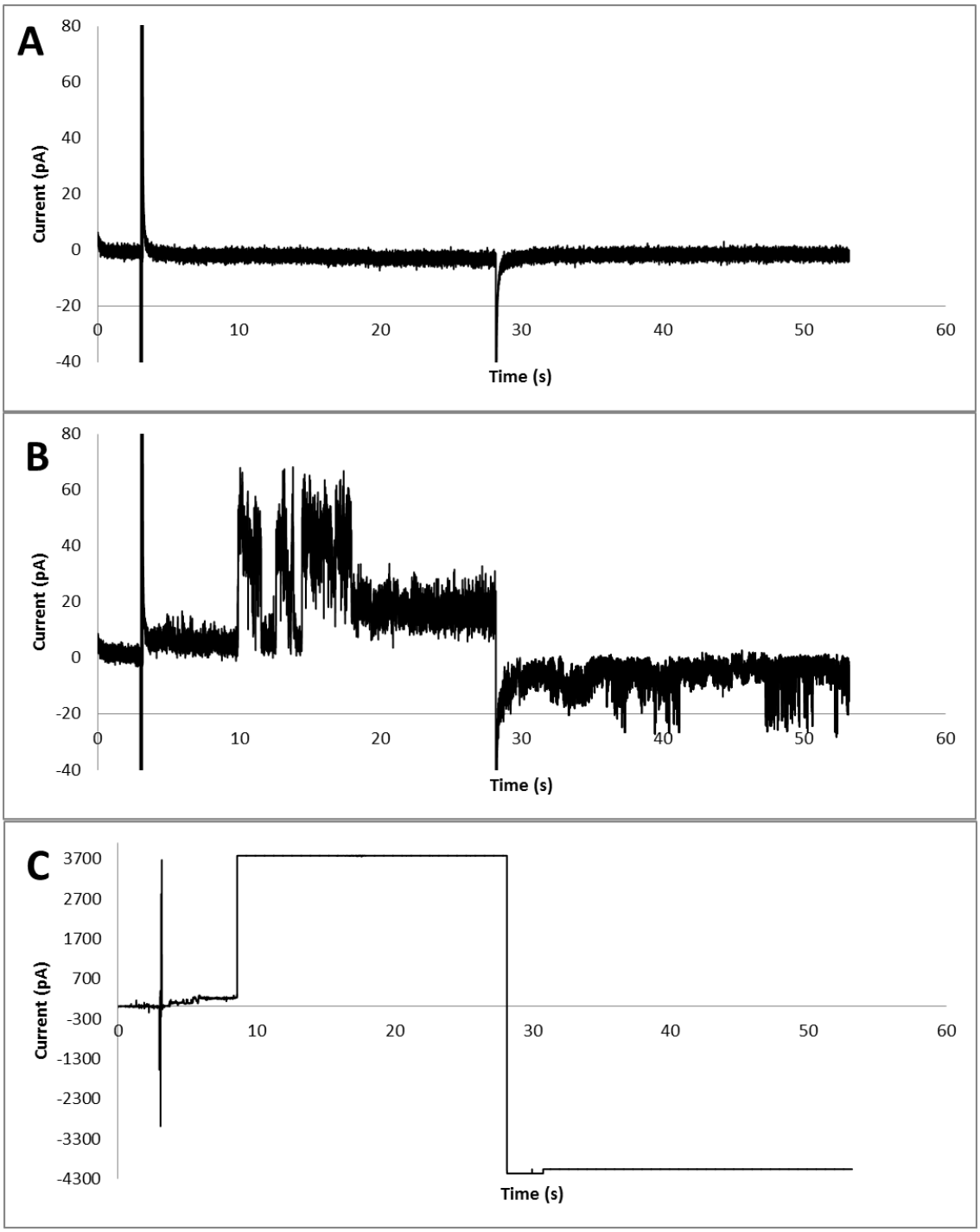

Figure 22: Cobalt Oxide (500 µg/ml): A: Typical trace of an experimental well with particle added. B: Typical trace of a control well with buffer added. C: Typical trace of an interaction event in an experimental well after particle has been added. D: Typical trace of a fusion event of an experimental well after particle has been added.

The particle exhibited very large current fluctuations, suggesting pores of substantial size were being formed. Fluctuations were as large as 60pA were observed as was transient pore formations. The current fluctuations were definitely stronger on the positive applied voltage portion of the protocol, however there many interactions on the negative side, suggesting the particle may not be completely voltage dependent.

Ionic strength experiment results are shown in the following table.

Table 14: Cobalt Oxide Ionic Strength Experimental Fusion Rates

Co_3O_4 (500 µg/ml)		
	Bilayer Fusion Rate	
Buffer	Control Wells	Experimental Wells
pH 4.5 5mM NaCl 5mM Tris-HCl	0/8	4/8
pH 4.5 80mM NaCl 5mM Tris-HCl	1/10	9/10
pH 4.5 1M NaCl 5mM Tris-HCl	0/7	0/8

Similar to the vast majority of particles, 80mM yielded the most fusions. Possible theories previously discussed.

pH results for cobalt oxide are shown in the table below, with intriguing results of many fusions at one pH and none at another pH.

Table 15: Cobalt Oxide pH Range Experimental Fusion Rates

Co_3O_4 (500 µg/ml)		
	Bilayer Fusion Rate	
Buffer	Control Wells	Experimental Wells
pH 4.5 80mM NaCl 5mM Tris-HCl	1/10	9/10
pH 7.0 80mM NaCl 5mM HEPES	0/10	0/10

Much like a switch being turned off, the nanoparticle was not able to fuse any bilayers at pH 7.0, a stark contrast after it had fused 90% if the bilayers at pH 4.5. This is a very interesting result, one that may warrant additional studies. Serum presence had a similar result.

Table 16: Cobalt Oxide Serum Experimental Fusion Rates

Co_3O_4 (500 µg/ml)		
	Bilayer Fusion Rate	
Condition	Control Wells	Experimental Wells
Buffer only (pH 4.5 80mM NaCl 5mM Tris-HCl)	1/10	9/10
Serum (with pH 7.0 80mM NaCl 5mM HEPES buffer)	0/7	2/8

There was a significant difference from the experiment with buffer only and the experiment with serum on one side of the bilayer. This means that any potential screening

resulting from the serum solution may have been occurring and resulted in the particle being unable to disrupt the bilayer.

4.6 Zinc Oxide (ZnO)

Zinc oxide was tested at 500 µg/ml, 100 µg/ml, and 50 µg/ml. Many particles were tested at 500 and 100 µg/ml but zinc was unique in regards to requiring a 50 µg/ml concentration in order to gather interaction data before a fusion event occurred.

Table 17: Zinc Oxide Initial Fusion Rate Experiments

ZnO pH 4.5 80mM NaCl 5mM Tris-HCl		
	Bilayer Fusion Rate	
Concentration	Control Wells	Experimental Wells
500 µg/ml	0/6	4/4
100 µg/ml	0/8	6/7
50 µg/ml	0/10	9/14

50 µg/ml was used for the remainder of tests. The figure below contains typical traces for zinc oxide.

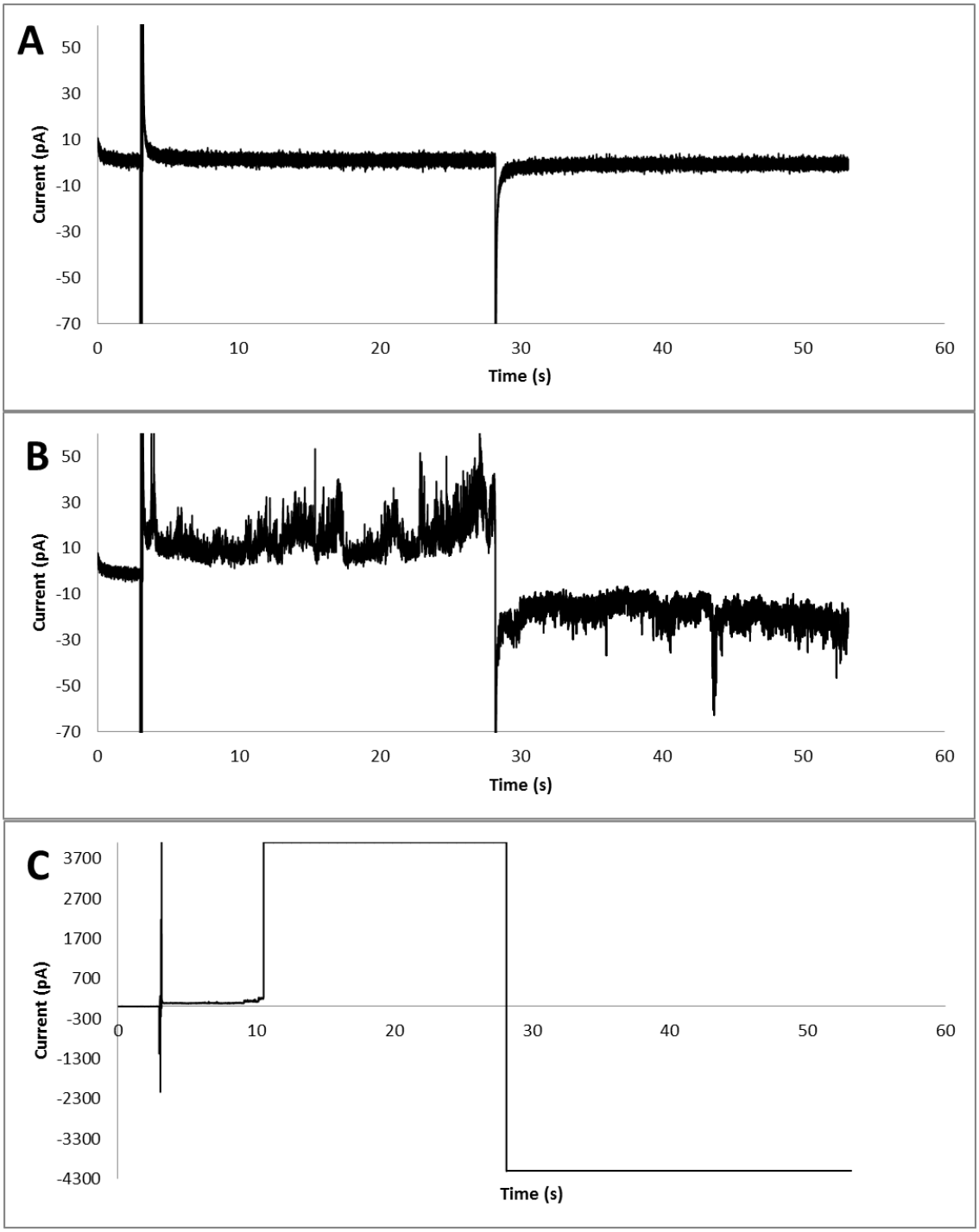

Figure 23: Zinc Oxide (50 µg/ml): A: Typical trace of an experimental well with particle added. B: Typical trace of a control well with buffer added. C: Typical trace of an interaction event in an experimental well after particle has been added. D: Typical trace of a fusion event of an experimental well after particle has been added.

Current fluctuations were up to 50pA. Pores were formed in both positive and negative applied voltages suggesting an independence of voltage sign.

For the ionic strength tests, 80mM yielded the most fusions, like most particles. Results are shown in the table below.

Table 18: Zinc Oxide Ionic Strength Experimental Fusion Rates

ZnO (50 µg/ml)		
	Bilayer Fusion Rate	
Buffer	Control Wells	Experimental Wells
pH 4.5 5mM NaCl 5mM Tris-HCl	0/8	2/8
pH 4.5 80mM NaCl 5mM Tris-HCl	0/10	9/14
pH 4.5 1M NaCl 5mM Tris-HCl	0/8	3/9

This particle reacted at all ionic strengths and at both pH experiments. It may be interesting to study whether there is any inherent quality or characteristic this particle may have that allows for it to interact and fuse bilayers in a variety of conditions at such a low concentration.

Table 19: Zinc Oxide pH Range Experimental Fusion Rates

ZnO (50 µg/ml)		
	Bilayer Fusion Rate	
Buffer	Control Wells	Experimental Wells
pH 4.5 80mM NaCl 5mM Tris-HCl	0/10	9/14
pH 7.0 80mM NaCl 5mM HEPES	0/9	4/5

The results of the serum environment tests also show a high fusion rate, however there is the caveat that the control wells also fused at a high rate, an unfortunate trait of the stability in serum conditions.

Table 20: Zinc Oxide Serum Experimental Fusion Rates

ZnO (50 µg/ml)		
	Bilayer Fusion Rate	
Condition	Control Wells	Experimental Wells
Buffer only (pH 4.5 80mM NaCl 5mM Tris-HCl)	0/10	9/14
Serum (with pH 7.0 80mM NaCl 5mM HEPES buffer)	4/11	5/13

4.7 Indium Oxide (In_2O_3)

Indium oxide, similar to the previous particles, was initially screened at various concentrations until a threshold was observed for bilayer fusions or interactions. These concentrations for this nanoparticle were 500 µg/ml and 100 µg/ml.

Table 21: Indium Oxide Initial Fusion Rate Experiments

In_2O_3 pH 4.5 80mM NaCl 5mM Tris-HCl		
	Bilayer Fusion Rate	
Concentration	Control Wells	Experimental Wells
500 µg/ml	4/21	16/20
100 µg/ml	3/11	5/10

Even at lower concentrations, such as 100 µg/ml, this particle proved to break the bilayers at a high percentage. The results collected from this data did not reveal any pore formation. The figures below is representative of typical traces for indium oxide experiments.

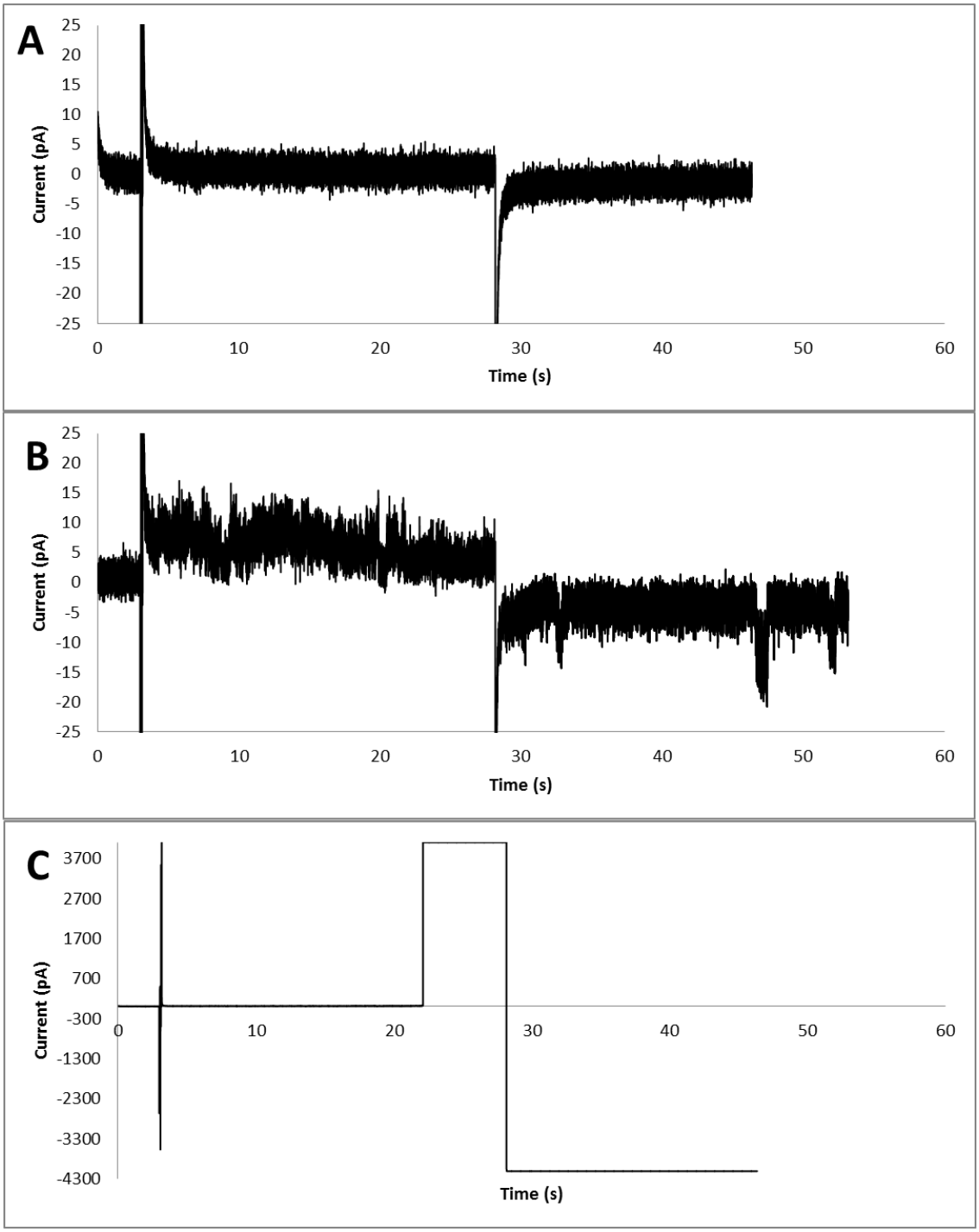

Figure 24: Indium Oxide (500 µg/ml): A: Typical trace of an experimental well with particle added. B: Typical trace of a control well with buffer added. C: Typical trace of an interaction event in an experimental well after particle has been added. D: Typical trace of a fusion event of an experimental well after particle has been added.

Indium oxide was an interesting nanoparticle, due to numerous transient pore formations. Pore formations occurred in both positive and negative voltages, with fluctuations of 15pA.

For the ionic strength experiments, the nanoparticle was tested at a concentration of 500 µg/ml the table below displays the fusion rates for each test for this nanoparticle.

Table 22: Indium Oxide Ionic Strength Experimental Fusion Rates

In_2O_3 (500 µg/ml)		
	Bilayer Fusion Rate	
Buffer	Control Wells	Experimental Wells
pH 4.5 5mM NaCl 5mM Tris-HCl	0/8	0/8
pH 4.5 80mM NaCl 5mM Tris-HCl	4/21	16/20

The results of the ionic strength test showed that there was a significant difference between the low ionic strength and the high ionic strengths.

Changes in pH were tested. pH 4.5 and pH 7.0 also showed a significant difference in fusion rates.

Table 23: Indium Oxide pH Range Experimental Fusion Rates

In_2O_3 (500 µg/ml)		
	Bilayer Fusion Rate	
Buffer	Control Wells	Experimental Wells
pH 4.5 80mM NaCl 5mM Tris-HCl	4/21	16/20
pH 7.0 80mM NaCl 5mM HEPES	0/10	0/10

The results of the different pH value tests, 4.5 and 7.0, yielded a significant difference. There was a strong affect from an acidic pH of 4.5 to a neutral pH of 7.0. The control bilayers were not reactive in terms of fusions and had little to no interactions. Perhaps this phenomenon can be attributed to the nanoparticles potential change in electrostatics.

Similar to the other nanoparticles, serum conditions had fewer fusions but also were limited in cohort size and were unstable in comparison to the other conditions making it difficult to draw strong conclusions on the topic.

Table 24: Indium Oxide Serum Experimental Fusion Rates

In_2O_3 (500 µg/ml)		
	Bilayer Fusion Rate	
Condition	Control Wells	Experimental Wells
Buffer only (pH 4.5 80mM NaCl 5mM Tris-HCl)	4/21	16/20
Serum (with pH 7.0 80mM NaCl 5mM HEPES buffer)	1/3	2/4

The control bilayers were more reactive in terms of fusions in comparison to previous test, likely due to instability caused by the serum, yet even with a potential extra amount of fusions for the experimental wells based simply on instability, the experimental wells in the serum experiments yielded significantly fewer fused bilayers.

4.8 Erbium Oxide (Er_2O_3)

Erbium oxide was initially screened at a particle concentration until a threshold was observed for bilayer fusions or interactions, this was determined to be the first concentration tested, 100 µg/ml at pH 4.5 with 80mM NaCl 5mM Tris-HCl buffer solution.

Table 25: Erbium Oxide Initial Fusion Rate Experiments

Er_2O_3 pH 4.5 80mM NaCl 5mM Tris-HCl		
	Bilayer Fusion Rate	
Concentration	Control Wells	Experimental Wells
100 µg/ml	0/8	9/10

Representative traces of erbium oxide can be found in the following figure. The figure shows a strong voltage dependence, with most interactions occurring on the positive portion of the trace. Transient pore formations were also observed, with current fluctuations of up to 25pA.

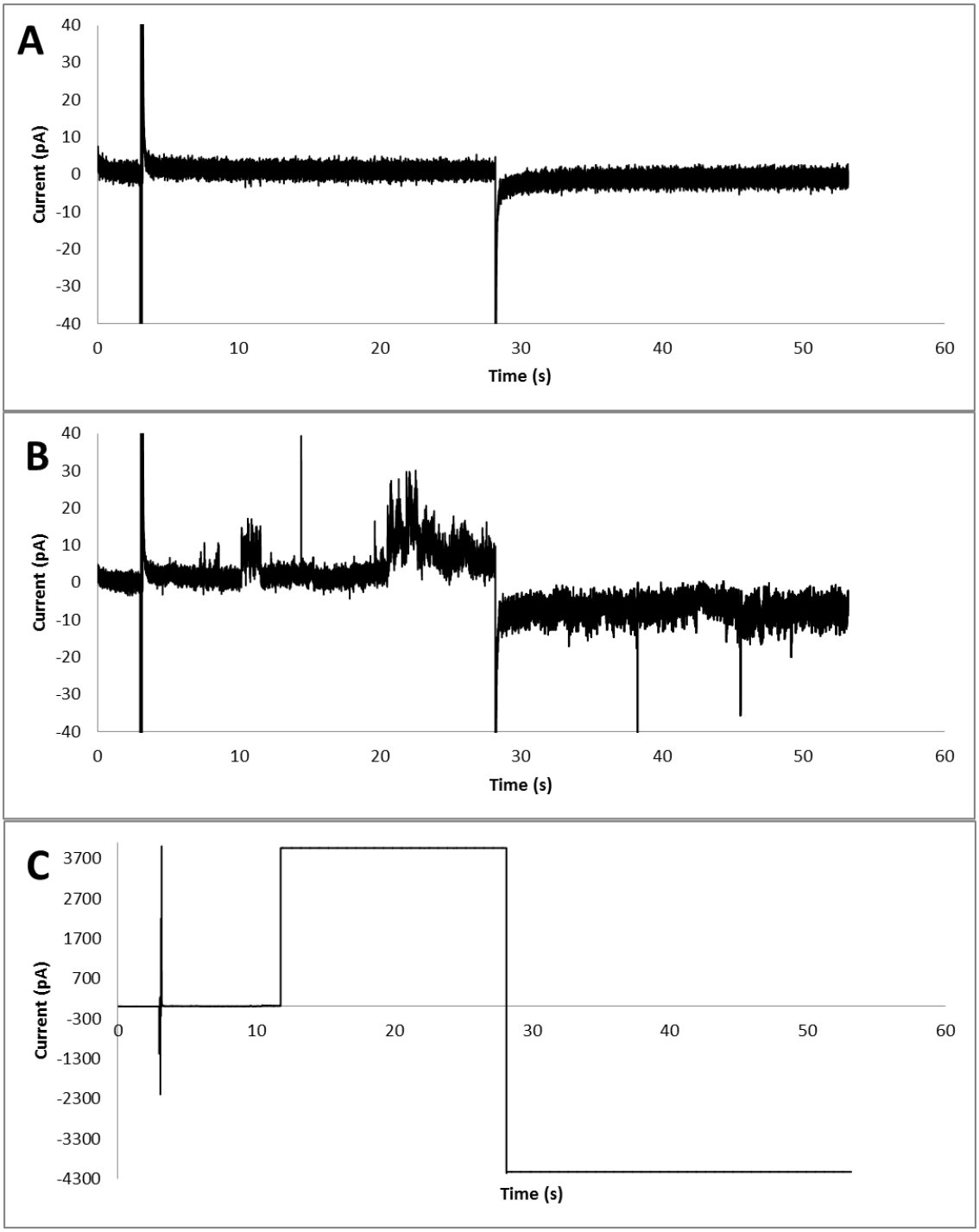

Figure 25: Erbium Oxide (100 µg/ml): A: Typical trace of an experimental well with particle added. B: Typical trace of a control well with buffer added. C: Typical trace of an interaction event in an experimental well after particle has been added. D: Typical trace of a fusion event of an experimental well after particle has been added.

Moving forward from these experiments, erbium oxide was tested at different ionic strengths with the same experimental protocol followed for two additional ionic strengths, with salt concentrations of 5mM NaCl and 1M NaCl.

Table 26: Erbium Oxide Ionic Strength Experimental Fusion Rates

Er_2O_3 (100 µg/ml)		
	Bilayer Fusion Rate	
Buffer	Control Wells	Experimental Wells
pH 4.5 5mM NaCl 5mM Tris-HCl	0/19	11/22
pH 4.5 80mM NaCl 5mM Tris-HCl	0/8	9/10
pH 4.5 1M NaCl 5mM Tris-HCl	1/19	9/19

The results of the ionic strength test showed that there was a significant difference between the middle ionic strength and the low ionic strength and high ionic strengths. There could be a relationship between the ionic strength and the particles ability to interact and fuse the bilayer. The control bilayers were not reactive in terms of fusions and had little to know interactions.

In addition to testing the effect of a change in ionic strength, changes in pH were tested. pH 4.5 and pH 7.0 was tested at 80mM NaCl at the previously determined experimental concentration. Tests with the experimental particles were conducted alongside control particles to ensure interactions and fusions were related to the particles.

The following results in the table below show the changes exhibited by the particle in the different conditions.

Table 27: Erbium Oxide pH Range Experimental Fusion Rates

Er_2O_3 (100 µg/ml)		
	Bilayer Fusion Rate	
Buffer	Control Wells	Experimental Wells
pH 4.5 80mM NaCl 5mM Tris-HCl	0/8	9/10
pH 7.0 80mM NaCl 5mM HEPES	1/5	7/11

The results of the different pH value tests, 4.5 and 7.0, didn't yield a significant difference. There wasn't much of an affect from an acidic pH of 4.5 to a neutral pH of 7.0. The control bilayers were barely reactive in terms of fusions and had few interations.

The FBS/alpha-MEM/streptomycin experiments were successful in showing that that particle was largely unreactive in serum conditions. The tests for this particle and condition had enough barely in the control conditions that were stable enough to provide confidence that the particle was unreactive.

Table 28: Erbium Oxide Serum Experimental Fusion Rates

Er_2O_3 (100 µg/ml)		
	Bilayer Fusion Rate	
Condition	Control Wells	Experimental Wells
Buffer only (pH 4.5 80mM NaCl 5mM Tris-HCl)	0/8	9/10
Serum (with pH 7.0 80mM NaCl 5mM HEPES buffer)	0/6	1/8

There was a significant difference from the experiment with buffer only and the experiment with serum on one side of the bilayer.

4.9 Europium Oxide (Eu_2O_3)

Europium oxide was initially screened at a particle concentration 100 µg/ml. As the table below shows, this nanoparticle exhibited strong interactions and high fusion rates at this concentration. Additional concentrations were not required due to the particle not immediately fusing and providing enough incite about its interactions with the bilayer.

Table 29: Europium Oxide Initial Fusion Rate Experiments

Eu_2O_3 pH 4.5 80mM NaCl 5mM Tris-HCl		
	Bilayer Fusion Rate	
Concentration	Control Wells	Experimental Wells
100 µg/ml	0/6	6/7

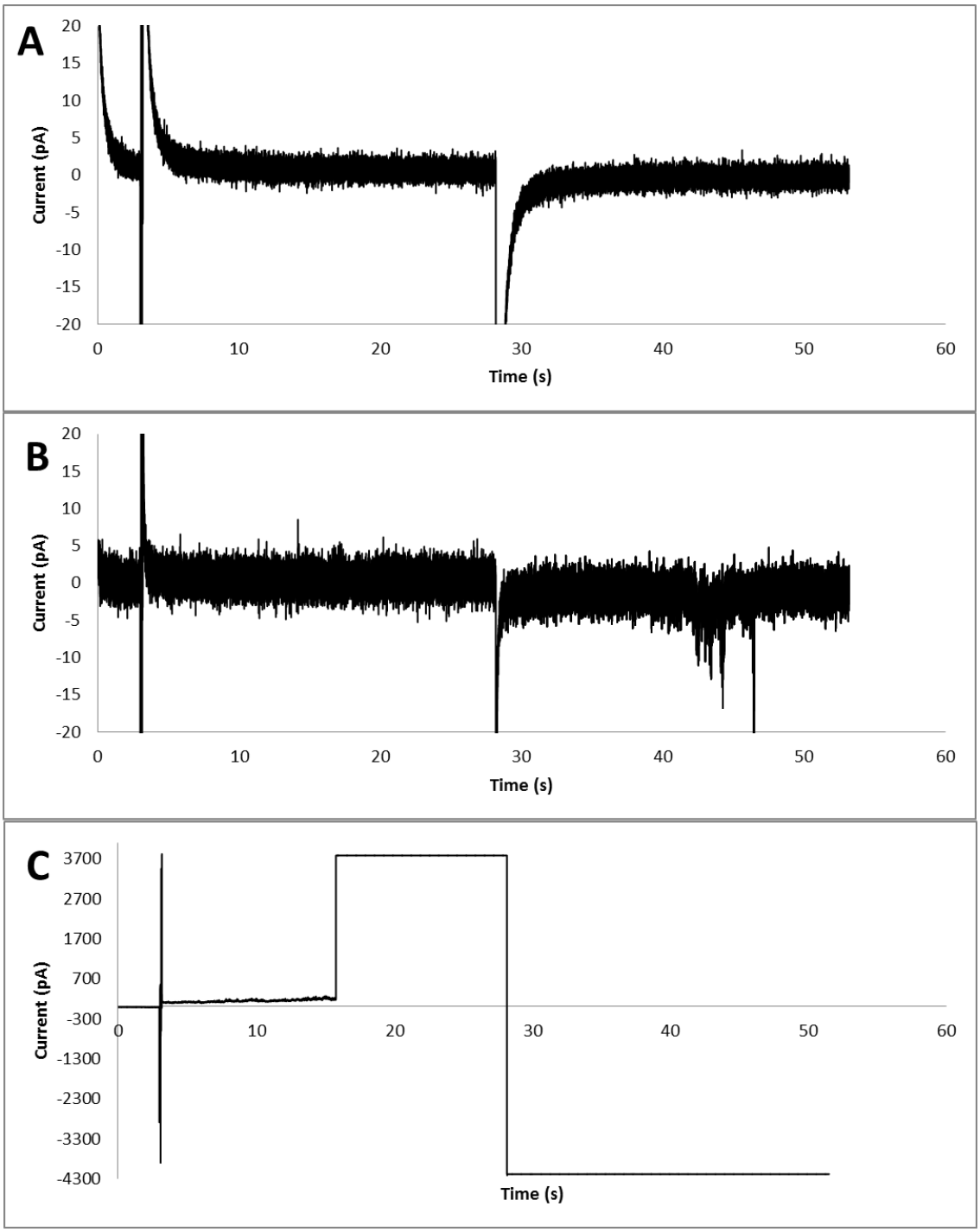

Figure 26: Europium Oxide (100µg/ml): A: Typical trace of an experimental well with particle added. B: Typical trace of a control well with buffer added. C: Typical trace of an interaction event in an experimental well after particle has been added. D: Typical trace of a fusion event of an experimental well after particle has been added.

The figure above shows that interactions with the bilayer were smaller current fluctuations of 10-15pA. The interactions occurred on the negative applied voltage portion of the protocol, suggesting possible voltage dependency.

For ionic strength tests, europium oxide was by far the most interesting nanoparticle, where it was very reactive at all ionic strength. It was proposed earlier that the high salt concentration was screening the charges and preventing the nanoparticles from having an interaction with the membrane. Any potential screening was not effective on europium oxide as 100% of the bilayers fused. Only 1/7 control bilayers fused, so the europium oxide data is significantly different. More research involving pore formations with europium oxide should be conducted.

Table 30: Europium Oxide Ionic Strength Experimental Fusion Rates

Eu_2O_3 (100 µg/ml)		
	Bilayer Fusion Rate	
Buffer	Control Wells	Experimental Wells
pH 4.5 5mM NaCl 5mM Tris-HCl	0/6	4/7
pH 4.5 80mM NaCl 5mM Tris-HCl	0/6	6/7
pH 4.5 1M NaCl 5mM Tris-HCl	1/7	11/11

Experiments involving pH provide another interesting wrinkle. The nanoparticle at pH 4.5 fused almost all bilayer but fused none at pH 7. This result was shared by many of the other nanoparticles, providing an interesting trend.

Table 31: Europium Oxide pH Range Experimental Fusion Rates

Eu_2O_3 (100 µg/ml)		
	Bilayer Fusion Rate	
Buffer	Control Wells	Experimental Wells
pH 4.5 80mM NaCl 5mM Tris-HCl	0/6	6/7
pH 7.0 80mM NaCl 5mM HEPES	0/4	0/5

FBS/alpha-MEM/streptomycin, also referred to as serum, had the following table of results from these experimental conditions.

Table 32: Europium Oxide Serum Experimental Fusion Rates

Eu_2O_3 (100 µg/ml)		
	Bilayer Fusion Rate	
Condition	Control Wells	Experimental Wells
Buffer only (pH 4.5 80mM NaCl 5mM Tris-HCl)	0/6	6/7
Serum (with pH 7.0 80mM NaCl 5mM HEPES buffer)	2/5	1/8

The bilayers were not stable enough and 40% of the controls actually fused. More tests will need to be conducted with serum before any conclusions can be drawn with this nanoparticle in that particular experimental condition.

4.10 Gadolinium Oxide (Gd_2O_3)

Lastly, gadolinium oxide was tested at 500 µg/ml and 100 µg/ml in the pH 4.5 buffer.

Table 33: Gadolinium Oxide Initial Fusion Rate Experiments

Gd_2O_3 pH 4.5 80mM NaCl 5mM Tris-HCl		
	Bilayer Fusion Rate	
Concentration	Control Wells	Experimental Wells
500 µg/ml	0/8	11/11
100 µg/ml	0/10	9/12

A concentration of 100 µg/ml, was determined to be the optimum concentration where bilayers fused but not before there was pore formations. Traces below are indicative of typical gadolinium oxide data.

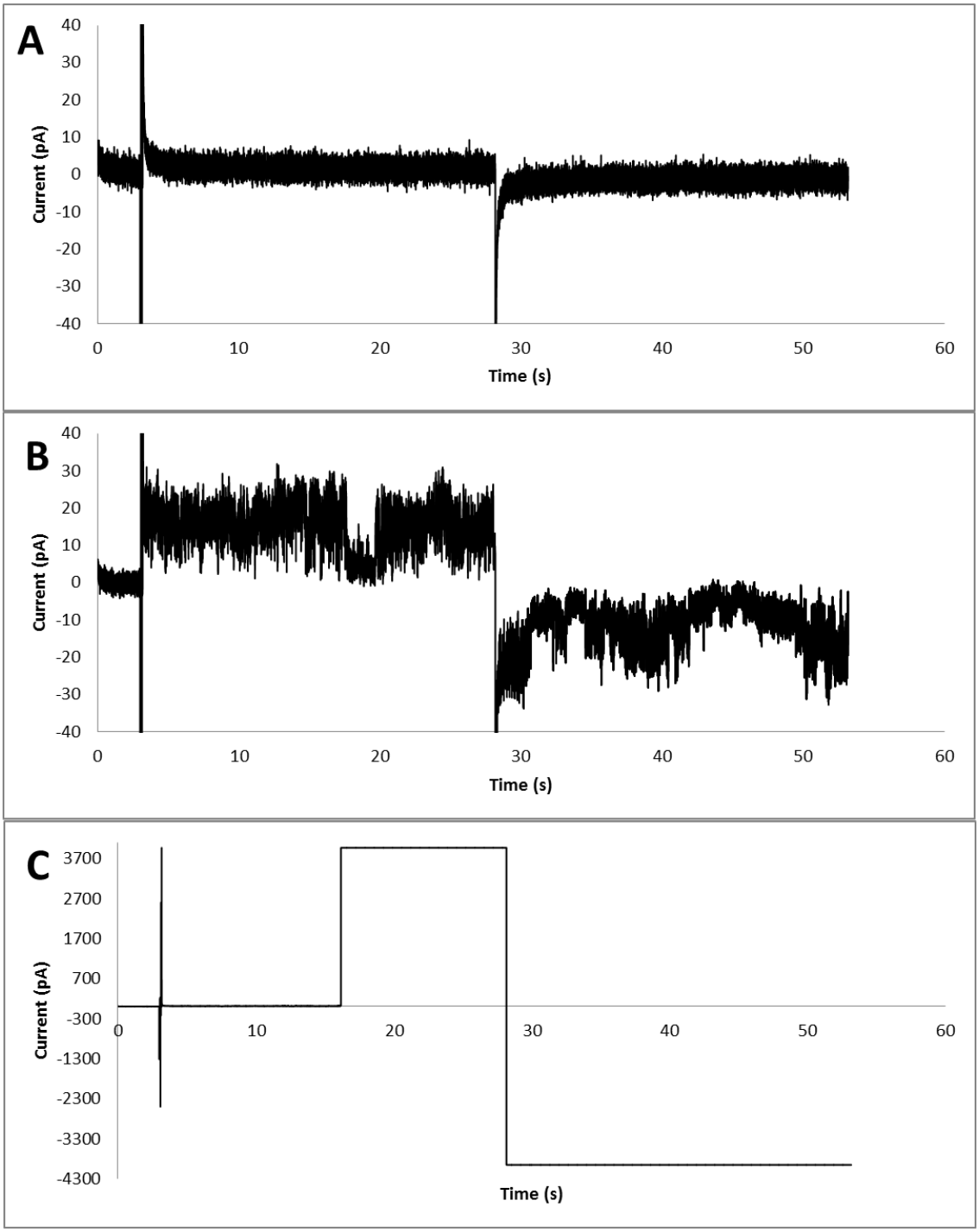

Figure 27: Gadolinium Oxide (100 µg/ml): A: Typical trace of an experimental well with particle added. B: Typical trace of a control well with buffer added. C: Typical trace of an interaction event in an experimental well after particle has been added. D: Typical trace of a fusion event of an experimental well after particle has been added.

Transient pore formations for several seconds were observed. Pores were formed in both positive and negative applied voltages, suggesting an independence of voltage. Fluctuations were up to 30pA in size.

Gadolinium oxide was reactive in all ionic strengths, a characteristic shared by only a few of the nanoparticles tested. More than half of the bilayers fused at the high salt concentration, suggesting that any charges the nanoparticle might exhibit were not being screened out.

Table 34: Gadolinium Oxide Ionic Strength Experimental Fusion Rates

Gd_2O_3 (100 µg/ml)		
	Bilayer Fusion Rate	
Buffer	Control Wells	Experimental Wells
pH 4.5 5mM NaCl 5mM Tris-HCl	0/9	7/8
pH 4.5 80mM NaCl 5mM Tris-HCl	0/10	9/12
pH 4.5 1M NaCl 5mM Tris-HCl	0/5	5/8

Changes in pH, 4.5 and pH 7.0, did not effect the fusion rate of gadolinium oxide much. The following results in the table below show the changes exhibited by the particle in the different conditions.

Table 35: Gadolinium Oxide pH Range Experimental Fusion Rates

Gd_2O_3 (100 µg/ml)		
	Bilayer Fusion Rate	
Buffer	Control Wells	Experimental Wells
pH 4.5 80mM NaCl 5mM Tris-HCl	0/8	9/10
pH 7.0 80mM NaCl 5mM HEPES	1/5	7/11

The results of the different pH value tests, 4.5 and 7.0, didn't yield a significant difference. The control bilayers had few interactions and fewer fusions.

Serum experiments were conducted for gadolinium oxide, and enough data was gathered to draw initial conclusions.

Table 36: Gadolinium Oxide Serum Experimental Fusion Rates

Gd_2O_3 (100 µg/ml)		
	Bilayer Fusion Rate	
Condition	Control Wells	Experimental Wells
Buffer only (pH 4.5 80mM NaCl 5mM Tris-HCl)	0/8	9/10
Serum (with pH 7.0 80mM NaCl 5mM HEPES buffer)	0/9	0/12

There was a significant difference from the experiment with buffer only and the experiment with serum on one side of the bilayer. Properties of the serum might have prevented gadolinium oxide from interacting with the bilayer.

Chapter 5: Future Work

There are many possible directions in which to continue future work. Initially more research in studying pore formations should be the next steps. A massive amount of data was collected in this work and more data analysis may provide more incites as to how and why one nanoparticle interacts with a lipid bilayer when another does not interact at all. Additional nanoparticles may be used to test theories that arise from the pore formation studies.

Another possible direction is investigating inverted head group lipids to study whether the interactions are purely related to the charge interactions between the lipids and the particles or if there are other potential forces that cause one particle to interact over another.

Appendix A: Protocols

A.1 Neutral Super Combo and Super Combo Lipid Preparation

Note: Three different lipid compositions are prepared and used in experiments. Neutral Super Combo and Super Combo plus BMP. The preparations for these two lipid compositions are largely the same, varying only with which individual components are added to the lipid composition.

The compositions, outlined in Table 37, Table 38, and Table 39 are shown below.

Table 37: Super Combo Plus BMP Lipid Composition

Super Combo Plus BMP Lipid Composition	
Lipid	Molar Ratio Composition
POPC	3
POPE	3
Cholesterol	3
POPS	1
Cerebroside	2
BMP	2

Table 38: Super Combo Lipid Composition

Super Combo Lipid Composition	
Lipid	Molar Ratio Composition
POPC	3
POPE	3
Cholesterol	3
POPS	1
Cerebroside	2

Table 39: Neutral Super Combo Lipid Composition

Neutral Super Combo Lipid Composition	
Lipid	Molar Ratio Composition
POPC	3
POPE	3
Cholesterol	3
Cerebroside	2

1. Vials of POPC, POPE, POPS, and BMP are shipped and stored in chloroform at a concentration of 10mg/ml and Cholesterol and Cerebroside are shipped and stored in powder form and are stored in a -20°C freezer.

2. Dilute a given amount of Cholesterol and Cerebroside powder in chloroform to 10mg/ml and 5mg/ml respectively.
3. Rinse a clean glass test tube with chloroform and evaporate with a gentle stream of argon gas.
4. Mix together lipids in the glass test tube with molar concentrations that align with Table 37, Table 38, and Table 39.
5. Dispense the mixed lipid solution into aliquots and backfill said aliquots with a gentle stream of argon gas
6. Cap and store lipid solution aliquots in a -20°C freezer until they are ready to be used.

A.2 Liposome and Lipid in Oil Preparation

1. Starting with a prepared lipid solution aliquot filled with chloroform, evaporate chloroform using argon gas.

   Note: For pH 4.5 without serum the lipid composition is Super Combo plus BMP, defined in Table 37. For pH 7.0 and 10.0 without serum the lipid composition is Super Combo defined in Table 38. For pH 7.0 with serum solutions, the lipid composition is Neutral Super Combo, defined in Table 39.
2. When the chloroform has been sufficiently evaporated, fill the vial/test tube/etc. with the appropriate pH and ionic strength buffer to a concentration of 10 mg/ml, hereafter referred to as liposome solution.
3. Sonicate this liposome solution for 30 seconds and then vortex the liposome solution for 30 seconds. Repeat this cycle a minimum of 5x, 7x recommended
4. Dilute the liposome solution, typically in a larger container, to a concentration of 250ug/ml with an addition of the buffer used in step 2. A test with 4 chips or 32 horizontal bilayers will require 16ml of diluted liposome solution.
5. Before use, vortex the diluted liposome solution for 30 seconds to ensure the solution is properly mixed before the experiment begins.
6. Evaporate an additional aliquot of lipid stored in chloroform is with a gentle stream of argon gas.
7. Add decane to the evaporated vial to a concentration of 10mg/ml, hereafter referred to as lipid in oil solution.

8. Place the lipid in oil solution on a shaker or tape to a vortexer for a minimum of 30 minutes.
9. The liposome and lipid in oil solutions are now ready to be used for the multichannel-horizontal bilayer platform.

A.3 Partition Hole Size and Quality Control Protocol

1. Using Delrin® film, the material used for partitions used in the multichannel array, cut sheets by hand to a size large enough to support a predefined batch of 30 chips.
2. Using a laser cutter and a two-piece die holder, cut partition hole sizes into the film in addition to the standard chip layout.
3. Choose partition hole sizes using a predetermined hole size programed in Adobe Illustrator®.
4. Verify each hole size using a multistep process, first involving the use of a light microscope to capture and image each partition hole. Before images are captured, settings must be adjusted for maximum contrast between the laser cut partition hole and the surrounding partition material. Document each image with well number, chip number, date of batch, and batch settings.
5. Transfer the images that have been recorded to a computer that has Matlab®.
6. Execute a Matlab® program to analyze the partition hole sizes. Calibrate the program by using an image with a scale bar and allow for accurate image sizes.
7. Once the program has been calibrated, input information such as wells ranges, chip ranges, and batch into the program's code before executing the code.
8. Execute the program to provide information on average hole size and standard deviation for each chip, row, and column. Additionally, the hole roundness should also be recorded.

9. To ensure quality control, review the statistics for discrepancies in the results in comparison to previous batches and any variability between rows and columns in the array within the batch.
10. Partitions that do not pass the initial quality control process are not utilized for experiments. For example, partitions that are not round or very jagged or at more than 10% away from a predetermined target size are not used.
11. For partitions that do pass initial quality control, the partitions are used to assemble chips.
12. Chips used in experiments are later analyzed for bilayer yield and failure characteristics. For example, at pH 7, it was discovered that the hole size needed to be larger than the hole size for pH 4.5 experiments.
13. Once experiments reach a certain success threshold of 70% or greater bilayer yield, the partition hole size characteristics are recorded and replaced for future experiments by following the quality control process.

A.4 Acrylic Chip Assembly Protocol

1. Each acrylic chip is composed of 3 acrylic parts, 2 layers of acrylic tape and one sheet of Delrin® film in which has a predetermined holes size cut via a laser cutter. These partition hole sizes are cut and verified via the Partition Hole Size and Quality Control Protocol. For pH 4.5, a diameter of 600-650 microns is optimal, and for pH 7.0 and 10.0, a diameter of 700-750 microns is optimal.
2. Glue the acrylic ladder parts and acrylic base parts together using fast-set acrylic glue.
3. Once the glue has properly cured, preferably overnight, assemble the chips starting with the top acrylic part being attached to the acrylic taped, which has been cut in the same pattern. Assemble the Delrin® film partitions between the top tape and the bottom tape. Finally attach the glued acrylic bottom part to this tape to finish the assembly.
4. Wash the assembled chips with decane for 30 minutes to ensure any possible contaminants from the burnt laser cut tape are eradicated from the chips.
5. Perform a methanol wash on the assembled chips to free the chips of any decane or other contaminants. Repeat this process three times with fifteen-minute intervals between each wash cycle.
6. After the last methanol wash, wash the chips with deionized water five times with five minutes between each wash cycle.
7. Dry each chip with pressurized air to remove as much water as possible.

8. Place dried chips in a vacuum container or desiccator to continue the drying process.
9. Chips that have been in the vacuum container or desiccator for more than four hours are ready to be used.

A.5 Multichannel Horizontal Bilayer Platform Protocol with Buffer Solution

1. Up to four 8 channel acrylic chips that are assembled, cleaned, dried, and appropriately sized can be used at once in the multichannel horizontal bilayer platform.
2. Prepare a liposome solution in the desired buffer by following Appendix A.2 Liposome and Lipid in Oil Preparation.
3. Prepare a lipid in oil solution in decane by following Appendix A.2 Liposome and Lipid in Oil Preparation.
4. Bleach silver electrodes for 30 minutes.
5. Wash bleached electrodes with methanol.
6. Following the methanol wash, wash the electrodes with deionized water.
7. Following the deionized water wash, dry the electrodes with pressurized air.
8. Add 450 microliters of liposome solution to the bottom of each well of each chip.
9. Add 25 microliters of lipid in oil solution to the top of each well of each chip.
10. Load and secure chips using tape to a four chip capacity docking station.
11. Insert cleaned electrodes into the secured chips arrays by inserting two electrodes into each well-channel array.
12. Start the Tecella© program and apply a voltage to each well-channel array.
13. Once fifteen minutes has passed, add 50 microliters of buffer to the top wells.
14. Evaluate channel for bilayer quality and characteristics.
15. For bilayers that have fused, turn off their respective channels.

16. For channels that do not have a bilayer, add 50 microliters to the bottom wells to add pressure to the bottom to encourage bilayers to form.
17. Evaluate the bilayer progress every 10 minutes and if necessary, added buffer in small increments, until a sufficient amount of bilayers have formed.
18. Prepare a particle of interest in a buffer solution at a predetermined concentration. The concentration is to be 10 times more concentrated than the experimental concentration desired.
19. Once a satisfactory number of bilayers are achieved, add the 5 microliters of the prepared particle solution to the top well for approximately half of the wells with bilayers.
20. Use the remaining wells with bilayers as controls. 5 microliters of buffer is added to the top in the same manner as the experimental wells.
21. The Tecella© is programmed to record traces of 60 seconds in length for two hours.
22. The researcher in charge of the experiment is to record any notes of interest in a word document. Notes of interest include interaction times, fusion times, and if there are any clear trends or unusual activity during the experiment.
23. Two hours after adding particle to the chips, the test is stopped. A summary of the experiment is recorded.

A.6 Serum Preparation

1. Prepare a solution comprising of 89% alpha-MEM, 10% Fetal Bovine Serum (FBS), and 1% Streptomycin. Thaw FBS and Streptomycin overnight when transferring from a -20°C freezer to a 0°C fridge.
2. Store prepared aliquots of alpha-MEM/FBS/Streptomycin in a -20°C freezer and transferred to 0°C fridge when needed.

A.7 Multichannel Horizontal Bilayer Platform Protocol with Serum Solution

1. Up to four 8 channel acrylic chips that are assembled, cleaned, dried, and appropriately sized can be used at once in the multichannel horizontal bilayer platform.
2. Prepare a liposome solution in the desired buffer by following Appendix A.2 Liposome and Lipid in Oil Preparation
3. Prepare a lipid in oil solution in decane by following Appendix A.2 Liposome and Lipid in Oil Preparation
4. Bleach silver electrodes for 30 minutes.
5. Wash bleached electrodes with methanol.
6. Following the methanol wash, wash the electrodes with deionized water.
7. Following the deionized water wash, dry the electrodes with pressurized air.
8. Add 450 microliters of liposome solution to the bottom of each well of each chip.
9. Add 25 microliters of lipid in oil solution to the top of each well of each chip.
10. Load and secure chips using tape to a four chip capacity docking station.
11. Insert cleaned electrodes into the secured chips arrays by inserting two electrodes into each well-channel array.
12. Start the Tecella© program and apply a voltage to each well-channel array.
13. Once fifteen minutes has passed, 50 microliters of serum solution is added to the top.
14. Evaluate channel for bilayer quality and characteristics.

15. For bilayers that have fused, turn off their respective channels.
16. For channels that do not have a bilayer, add 50 microliters to the bottom wells to add pressure to the bottom to encourage bilayers to form.
17. Evaluate the bilayer progress every 10 minutes and if necessary, added buffer in small increments, until a sufficient amount of bilayers have formed.
18. A particle of interest is prepared in a serum solution at a predetermined concentration. The concentration is to be 10 times more concentrated than the experimental concentration desired.
19. Once a satisfactory number of bilayers are achieved, add the 5 microliters of the prepared particle solution to the top well for approximately half of the wells with bilayers.
20. Use the remaining wells with bilayers as controls. 5 microliters of buffer is added to the top in the same manner as the experimental wells.
21. The Tecella© is programmed to record traces of 60 seconds in length for two hours.
22. The researcher in charge of the experiment is to record any notes of interest in a word document. Notes of interest include interaction times, fusion times, and if there are any clear trends or unusual activity during the experiment.
23. Two hours after adding particle to the chips, the test is stopped. A summary of the experiment is recorded.

A.8 Painted Bilayer Preparation and Protocol

1. Prepare lipid in oil solution in accordance with Appendix A.2 Liposome and Lipid in Oil Preparation, with a predetermined lipid or lipid mixture at a concentration of 20 mg/ml.
2. The painted bilayer apparatus is comprised of the following components: a PTFE cup, a part capable of working as a docking-like station for the cup and a compartment of outside buffer, and two silver wire electrode which are connected to an amplifier and a ground respectively.
3. Thoroughly clean the PTFE cup by a wash cycle using chloroform, ethanol, acetone, methanol, and deionized water. Skipping one of these steps may lead to less than favorable results.
4. Thoroughly dry the PTFE cup with a high-pressure stream of air.
5. Clean the cup docking station part with methanol and deionized water before it is dried with a high-pressure stream of air.
6. Dip a glass rod in the lipid in oil solution to pre-coat the hole of the PTFE cup.
7. Place the pre-coated cup in the complimentary docking station part and fill with 1mL of buffer solution.
8. Add 1mL of buffer solution to the outside well compartment to achieve equal pressure on both sides of the hole of the PTFE cup.
9. Place one electrode in solution on each side of the cup and apply a voltage.

10. Insert the glass rod into the outside well glide the glass rod over the hole to remove any oil and aide the bilayer to form. This lends to the naming of this process as painting.
11. If a bilayer does not form after several painting strokes, additional lipid in oil solution may be used. This can be accomplished by dipping the glass rod into the lipid in oil solution.
12. Once a bilayer is formed, add particle to one side of the cup, typically the inside.
13. Recorded data to observe interactions with the bilayer, if any.
14. Once the bilayer fuses it may be repainted or the cup may be washed to repeat the process.

References

[1] Zimmerberg, Joshua, and Michael M. Kozlov. "How proteins produce cellular membrane curvature." *Nature Reviews Molecular Cell Biology* 7.1 (2006): 9-19.

[2] Lelièvre, Sophie, Valerie M. Weaver, and Mina J. Bissell. "Extracellular matrix signaling from the cellular membrane skeleton to the nuclear skeleton: a model of gene regulation." *Recent progress in hormone research* 51 (1996): 417.

[3] Ashford, Thomas P., and Keith R. Porter. "Cytoplasmic components in hepatic cell lysosomes." *The Journal of cell biology* 12.1 (1962): 198-202.

[4] Loewenstein, WERNER R. "Junctional intercellular communication: the cell-to-cell membrane channel." *Physiological Reviews* 61.4 (1981): 829-913.

[5] Davson, Hugh, and James Frederic Danielli. "The permeability of natural membranes." *The permeability of natural membranes.* (1943).

[6] Singer, S. J., and Garth L. Nicolson. "The fluid mosaic model of the structure of cell membranes." *Day and Good Membranes and viruses in immunopathology* (1972): 7-47.

[7] Hanke, Wolfgang, and W. R. Schulue. *Planar lipid bilayers: methods and applications*. Academic Press, 2012.

[8] Kohler, Susan J., and Melvin P. Klein. "Orientation and dynamics of phospholipid head groups in bilayers and membranes determined from phosphorus-31 nuclear magnetic resonance chemical shielding tensors." *Biochemistry* 16.3 (1977): 519-526.

[9] Stigter, Dirk, and Ken A. Dill. "Lateral interactions among phospholipid head groups at the heptane/water interface." *Langmuir* 4.1 (1988): 200-209.

[10] Nagle, John F., and Stephanie Tristram-Nagle. "Structure of lipid bilayers." *Biochimica et Biophysica Acta (BBA)-Reviews on Biomembranes* 1469.3 (2000): 159-195.

[11] Sundava, David E. “Chapter 3.” *Life, the Science of Biology.* 8th ed. Sunderland, MA: Sinauer Associates;, 2008. 124. Print.

[12] Ide, Toru, and Takehiko Ichikawa. "A novel method for artificial lipid-bilayer formation." *Biosensors and Bioelectronics* 21.4 (2005): 672-677.

[13] Hirano-Iwata, Ayumi, Michio Niwano, and Masao Sugawara. "The design of molecular sensing interfaces with lipid-bilayer assemblies." *TrAC Trends in Analytical Chemistry* 27.6 (2008): 512-520.

[14] Mueller, Paul, et al. "Reconstitution of cell membrane structure in vitro and its transformation into an excitable system." *Nature* 194 (1962): 979-980.

[15] Alvarez, Osvaldo. "How to set up a bilayer system." *Ion channel reconstitution*. Springer US, 1986. 115-130.

[16] Mayer, Michael, et al. "Microfabricated teflon membranes for low-noise recordings of ion channels in planar lipid bilayers." *Biophysical journal* 85.4 (2003): 2684-2695.

[17] Han, Xiaojun, et al. "Nanopore Arrays for Stable and Functional Free-Standing Lipid Bilayers." *Advanced Materials* 19.24 (2007): 4466-4470.

[18] Florin, E-L., and H. E. Gaub. "Painted supported lipid membranes." *Biophysical journal* 64.2 (1993): 375.

[19] Montal, M., and P. Mueller. "Formation of bimolecular membranes from lipid monolayers and a study of their electrical properties." *Proceedings of the National Academy of Sciences* 69.12 (1972): 3561-3566.

[20] Anzai, Kazunori, et al. "Quantitative comparison of two types of planar lipid bilayers—folded and painted—with respect to fusion with vesicles." *Journal of biochemical and biophysical methods* 48.3 (2001): 283-291.

[21] Hanke, Wolfgang. "Incorporation of ion channels by fusion." *Ion channel reconstitution*. Springer US, 1986. 141-153.

[22] White, Stephen H. "The physical nature of planar bilayer membranes." *Ion Channel Reconstitution*. Springer US, 1986. 3-35.

[23] Le Pioufle, Bruno, et al. "Lipid bilayer microarray for parallel recording of transmembrane ion currents." *Analytical chemistry* 80.1 (2008): 328-332.

[24] Suzuki, Hiroaki, Bruno Le Pioufle, and Shoji Takeuhci. "Ninety-six-well planar lipid bilayer chip for ion channel recording fabricated by hybrid stereolithography." *Biomedical microdevices* 11.1 (2009): 17-22.

[25] Funakoshi, Kei, Hiroaki Suzuki, and Shoji Takeuchi. "Lipid bilayer formation by contacting monolayers in a microfluidic device for membrane protein analysis." *Analytical chemistry* 78.24 (2006): 8169-8174.

[26] Tsofina, L. M., E. A. Liberman, and A. V. Babakov. "Production of bimolecular protein-lipid membranes in aqueous solution." (1966): 681-683.

[27] Holden, Matthew A., David Needham, and Hagan Bayley. "Functional bionetworks from nanoliter water droplets." *Journal of the American Chemical Society* 129.27 (2007): 8650-8655.

[28] Bayley, Hagan, et al. "Droplet interface bilayers." *Molecular BioSystems* 4.12 (2008): 1191-1208.

[29] Aghdaei, Sara, et al. "Formation of artificial lipid bilayers using droplet dielectrophoresis." *Lab on a Chip* 8.10 (2008): 1617-1620.

[30] Poulos, Jason L., et al. "Electrowetting on dielectric-based microfluidics for integrated lipid bilayer formation and measurement." *Applied Physics Letters* 95.1 (2009): 013706.

[31] Poulos, Jason L., et al. "Ion channel and toxin measurement using a high throughput lipid membrane platform." *Biosensors and Bioelectronics* 24.6 (2009): 1806-1810.

[32] Kawano, Ryuji, et al. "Automated parallel recordings of topologically identified single ion channels." *Scientific reports* 3 (2013).

[33] Zagnoni, Michele, Mairi E. Sandison, and Hywel Morgan. "Microfluidic array platform for simultaneous lipid bilayer membrane formation." *Biosensors and Bioelectronics* 24.5 (2009): 1235-1240.

[34] Beck, Valeri, et al. "A new automated technique for the reconstitution of hydrophobic proteins into planar bilayer membranes. Studies of human recombinant uncoupling protein 1." *Biochimica et Biophysica Acta (BBA)-Bioenergetics* 1757.5 (2006): 474-479.

[35] Poulos, Jason L., et al. "Ion channel and toxin measurement using a high throughput lipid membrane platform." *Biosensors and Bioelectronics* 24.6 (2009): 1806-1810.

[36] Lu, Bin, Gayane Kocharyan, and Jacob J. Schmidt. "Lipid bilayer arrays: Cyclically formed and measured." *Biotechnology journal* 9.3 (2014): 446-451.

[37] Sanchez, Florence, and Konstantin Sobolev. "Nanotechnology in concrete–a review." *Construction and Building Materials* 24.11 (2010): 2060-2071.

[38] Farokhzad, Omid C., and Robert Langer. "Impact of nanotechnology on drug delivery." *ACS nano* 3.1 (2009): 16-20.

[39] Arayne, M. Saeed, and N. Sultana. "Review: nanoparticles in drug delivery for the treatment of cancer." *Pakistan journal of pharmaceutical sciences* 19.3 (2006): 258-268.

[40] Panyam, Jayanth, and Vinod Labhasetwar. "Biodegradable nanoparticles for drug and gene delivery to cells and tissue." *Advanced drug delivery reviews* 55.3 (2003): 329-347.

[41] Gao, Jinhao, et al. "Multifunctional yolk– shell nanoparticles: A potential MRI contrast and anticancer agent." *Journal of the American Chemical Society* 130.35 (2008): 11828-11833.

[42] Armentano, I., et al. "Biodegradable polymer matrix nanocomposites for tissue engineering: a review." *Polymer Degradation and Stability* 95.11 (2010): 2126-2146.

[43] Petoral Jr, Rodrigo M., et al. "Synthesis and characterization of Tb3+-doped Gd2O3 nanocrystals: a bifunctional material with combined fluorescent labeling and MRI contrast agent properties." *The Journal of Physical Chemistry C* 113.17 (2009): 6913-6920.

[44] Taton, T. Andrew, Chad A. Mirkin, and Robert L. Letsinger. "Scanometric DNA array detection with nanoparticle probes." *Science* 289.5485 (2000): 1757-1760.

[45] Salata, Oleg V. "Applications of nanoparticles in biology and medicine." *Journal of nanobiotechnology* 2.1 (2004): 3.

[46] Albanese, Alexandre, Peter S. Tang, and Warren CW Chan. "The effect of nanoparticle size, shape, and surface chemistry on biological systems." *Annual review of biomedical engineering* 14 (2012): 1-16.

[47] Endo, Tatsuro, et al. "Multiple label-free detection of antigen-antibody reaction using localized surface plasmon resonance-based core-shell structured nanoparticle layer nanochip." *Analytical Chemistry* 78.18 (2006): 6465-6475.

[48] De Jong, Wim H., and Paul JA Borm. "Drug delivery and nanoparticles: applications and hazards." *International journal of nanomedicine* 3.2 (2008): 133.

[49] Muller, Rainer H., and Cornelia M. Keck. "Challenges and solutions for the delivery of biotech drugs–a review of drug nanocrystal technology and lipid nanoparticles." *Journal of biotechnology* 113.1 (2004): 151-170.

[50] Lundqvist, Martin. "Nanoparticles: tracking protein corona over time." *Nature nanotechnology* 8.10 (2013): 701-702.

[51] Stoeva, Savka I., et al. "Multiplexed detection of protein cancer markers with biobarcoded nanoparticle probes." *Journal of the American Chemical Society* 128.26 (2006): 8378-8379.

[52] Salata, Oleg V. "Applications of nanoparticles in biology and medicine." *Journal of nanobiotechnology* 2.1 (2004): 3.

[53] Kango, Sarita, et al. "Surface modification of inorganic nanoparticles for development of organic–inorganic nanocomposites—A review." *Progress in Polymer Science* 38.8 (2013): 1232-1261.

[54] Laurent, Sophie, et al. "Magnetic iron oxide nanoparticles: synthesis, stabilization, vectorization, physicochemical characterizations, and biological applications." *Chemical reviews* 108.6 (2008): 2064-2110.

[55] Liu, Juewen, et al. "Electrostatically mediated liposome fusion and lipid exchange with a nanoparticle-supported bilayer for control of surface charge, drug containment, and delivery." *Journal of the American Chemical Society* 131.22 (2009): 7567-7569.

[56] Khanjani, Somaye, and Ali Morsali. "Synthesis and characterization of lanthanum oxide nanoparticles from thermolysis of nanostructured supramolecular compound." *Journal of Molecular Liquids* 153.2 (2010): 129-132.

[57] Bouzigues, Cedric, Thierry Gacoin, and Antigoni Alexandrou. "Biological applications of rare-earth based nanoparticles." *ACS nano* 5.11 (2011): 8488-8505.

[58] Yang, Jiancan, Zuoren Nie, and Yiman Wang. "Microstructure and emission ability of rare earth oxides doped molybdenum cathodes." *Applied surface science* 215.1 (2003): 87-95.

[59] Zarur, Andrey J., and Jackie Y. Ying. "Reverse microemulsion synthesis of nanostructured complex oxides for catalytic combustion." *nature* 403.6765 (2000): 65-67.

[60] Xu, Can, and Xiaogang Qu. "Cerium oxide nanoparticle: a remarkably versatile rare earth nanomaterial for biological applications." *NPG Asia Materials* 6.3 (2014): e90.

[61] Wason, Melissa S., and Jihe Zhao. "Cerium oxide nanoparticles: potential applications for cancer and other diseases." *American journal of translational research* 5.2 (2013): 126.

[62] Celardo, Ivana, et al. "Pharmacological potential of cerium oxide nanoparticles." *Nanoscale* 3.4 (2011): 1411-1420.

[63] Xu, Can, et al. "Nanoceria-Triggered Synergetic Drug Release Based on CeO2-Capped Mesoporous Silica Host–Guest Interactions and Switchable Enzymatic Activity and Cellular Effects of CeO2." *Advanced healthcare materials* 2.12 (2013): 1591-1599.

[64] Li, Meng, et al. "Cerium oxide caged metal chelator: anti-aggregation and anti-oxidation integrated H 2 O 2-responsive controlled drug release for potential Alzheimer's disease treatment." *Chemical Science* 4.6 (2013): 2536-2542.

[65] Rahnama, Ahmad, and Mehrnaz Gharagozlou. "Preparation and properties of semiconductor CuO nanoparticles via a simple precipitation method at different reaction temperatures." *Optical and Quantum Electronics* 44.6-7 (2012): 313-322.

[66] Jiang, Liao-Chuan, and Wei-De Zhang. "A highly sensitive nonenzymatic glucose sensor based on CuO nanoparticles-modified carbon nanotube electrode." *Biosensors and Bioelectronics* 25.6 (2010): 1402-1407.

[67] Song, Min-Jung, Sung Woo Hwang, and Dongmok Whang. "Non-enzymatic electrochemical CuO nanoflowers sensor for hydrogen peroxide detection." *Talanta* 80.5 (2010): 1648-1652.

[68] Ren, Guogang, et al. "Characterisation of copper oxide nanoparticles for antimicrobial applications." *International journal of antimicrobial agents* 33.6 (2009): 587-590.

[69] Ruparelia, Jayesh P., et al. "Strain specificity in antimicrobial activity of silver and copper nanoparticles." *Acta Biomaterialia* 4.3 (2008): 707-716.

[70] Jiao, Feng, and Heinz Frei. "Nanostructured Cobalt Oxide Clusters in Mesoporous Silica as Efficient Oxygen-Evolving Catalysts." *Angewandte Chemie International Edition* 48.10 (2009): 1841-1844.

[71] Cao, An-Min, et al. "Hierarchically structured cobalt oxide (Co3O4): the morphology control and its potential in sensors." *The Journal of Physical Chemistry B* 110.32 (2006): 15858-15863.

[72] Ryu, Jungki, et al. "Synthesis of diphenylalanine/cobalt oxide hybrid nanowires and their application to energy storage." *ACS nano* 4.1 (2009): 159-164.

[73] Llusar, M., et al. "Colour analysis of some cobalt-based blue pigments." *Journal of the European Ceramic Society* 21.8 (2001): 1121-1130.

[74] Michael, Sheree E. Crossa Brian Innesb, S. Robertsa Takuya Tsuzukib, and Terry A. Robertsonc Paul McCormickb. "Human skin penetration of sunscreen nanoparticles: in-vitro assessment of a novel micronized zinc oxide formulation." *Skin Pharmacol Physiol* 20 (2007): 148-154.

[75] Godfrey, H. R., et al. "A randomized clinical trial on the treatment of oral herpes with topical zinc oxide/glycine." *Alternative therapies in health and medicine* 7.3 (2000): 49-56.

[76] Jagadish, Chennupati, and Stephen J. Pearton, eds. *Zinc oxide bulk, thin films and nanostructures: processing, properties, and applications*. Elsevier, 2011.

[77] Yamamoto, Osamu. "Influence of particle size on the antibacterial activity of zinc oxide." *International Journal of Inorganic Materials* 3.7 (2001): 643-646.

[78] Rasmussen, John W., et al. "Zinc oxide nanoparticles for selective destruction of tumor cells and potential for drug delivery applications." *Expert opinion on drug delivery* 7.9 (2010): 1063-1077.

[79] Chen, Po-Chiang, et al. "High-performance single-crystalline arsenic-doped indium oxide nanowires for transparent thin-film transistors and active matrix organic light-emitting diode displays." *ACS nano* 3.11 (2009): 3383-3390.

[80] Dehuff, N. L., et al. "Transparent thin-film transistors with zinc indium oxide channel layer." *Journal of Applied Physics* 97.6 (2005): 064505-064505.

[81] Zhang, D., et al. "Ultraviolet photodetection properties of indium oxide nanowires." *Applied Physics A* 77.1 (2003): 163-166.

[82] Yamaura, Hiroyuki, et al. "Indium oxide-based gas sensor for selective detection of CO." *Sensors and Actuators B: Chemical* 36.1 (1996): 325-332.

[83] Radziuk, Darya, et al. "Ultrasonic approach for formation of erbium oxide nanoparticles with variable geometries." *Langmuir* 27.23 (2011): 14472-14480.

[84] El-Mallawany, R., et al. "Study of luminescence properties of Er 3+-ions in new tellurite glasses." *Optical Materials* 26.3 (2004): 267-270.

[85] Mahnke, M., et al. "Aluminum oxide doped with erbium, titanium and chromium for active integrated optical applications." *AEU-International Journal of Electronics and Communications* 55.5 (2001): 342-348.

[86] Feng, Jun, et al. "Functionalized europium oxide nanoparticles used as a fluorescent label in an immunoassay for atrazine." *Analytical Chemistry* 75.19 (2003): 5282-5286.

[87] Bazzi, R., et al. "Synthesis and properties of europium-based phosphors on the nanometer scale: Eu 2 O 3, Gd 2 O 3: Eu, and Y 2 O 3: Eu." *Journal of colloid and interface science* 273.1 (2004): 191-197.

[88] Park, Ja Young, et al. "Paramagnetic ultrasmall gadolinium oxide nanoparticles as advanced T 1 MRI contrast agent: account for large longitudinal relaxivity, optimal particle diameter, and in vivo T 1 MR images." *ACS nano* 3.11 (2009): 3663-3669.

[89] McDonald, Michael A., and Kenneth L. Watkin. "Small particulate gadolinium oxide and gadolinium oxide albumin microspheres as multimodal contrast and therapeutic agents." *Investigative radiology* 38.6 (2003): 305-310.

[90] Iversen, Tore-Geir, Tore Skotland, and Kirsten Sandvig. "Endocytosis and intracellular transport of nanoparticles: present knowledge and need for future studies." Nano Today 6.2 (2011): 176-185.